

Generalized Bayesian Multidimensional Scaling and Model Comparison

Jiarui Zhang*, Jiguo Cao* and Liangliang Wang*

Abstract. Multidimensional scaling (MDS) is widely used to reconstruct a low-dimensional representation of high-dimensional data while preserving pairwise distances. However, Bayesian MDS approaches based on Markov chain Monte Carlo (MCMC) face challenges in model generalization and comparison. To address these limitations, we propose a generalized Bayesian multidimensional scaling (GBMDS) framework that accommodates non-Gaussian errors and diverse dissimilarity metrics for improved robustness. We develop an adaptive annealed Sequential Monte Carlo (ASMC) algorithm for Bayesian inference, leveraging an annealing schedule to enhance posterior exploration and computational efficiency. The ASMC algorithm also provides a nearly unbiased marginal likelihood estimator, enabling principled Bayesian model comparison across different error distributions, dissimilarity metrics, and dimensional choices. Using synthetic and real data, we demonstrate the effectiveness of the proposed approach. Our results show that ASMC-based GBMDS achieves superior computational efficiency and robustness compared to MCMC-based methods under the same computational budget. The implementation of our proposed method and applications are available at <https://github.com/SFU-Stat-ML/GBMDS>.

Keywords: Sequential Monte Carlo, dimension reduction, adaptive inference, robustness, skewness, visualization.

1 Introduction

Multidimensional scaling (MDS) is a dimension reduction technique that represents objects as points in a lower-dimensional space based on a given set of pairwise dissimilarities between objects. The goal is to preserve the relative distance from the original high-dimensional space. MDS is widely applied across various fields, such as psychology, social science, and genomics, to uncover hidden patterns, explore relationships in complex datasets, and facilitate visualization. By transforming high-dimensional data into a spatial representation, typically two or three dimensions, MDS enables researchers to detect clusters, trends, and structures that might otherwise be difficult to interpret. It also supports exploratory data analysis by identifying the principal dimensions underlying dissimilarities, making it a valuable tool for both data visualization and statistical inference.

MDS methods are broadly categorized into metric and non-metric approaches. Metric MDS assumes that dissimilarities represent numerical distances and satisfy metric properties such as symmetry and the triangle inequality. It is particularly appropriate

*Department of Statistics and Actuarial Science, Simon Fraser University, Canada. jiarui_zhang@sfu.ca, jiguo_cao@sfu.ca, lwa68@sfu.ca

when the underlying data structure follows Euclidean geometry or when a specific distance function, such as the Euclidean or Mahalanobis distance, is justified. Non-metric MDS, on the other hand, is designed for ordinal or rank-based dissimilarities, where the absolute values of distances are not meaningful, and only the relative ordering of dissimilarities matters. This method is widely used in applications where dissimilarities do not adhere to strict metric properties, such as in psychological or perceptual studies. Despite differences in assumptions, both MDS approaches aim to embed high-dimensional data into a lower-dimensional space while preserving the original similarity structure as faithfully as possible. Our study primarily focuses on metric MDS. For a comprehensive review of modern MDS methods, see [Borg and Groenen \(2005\)](#).

Classical multidimensional scaling (CMDS), introduced by [Torgerson \(1952\)](#), is a foundational method for metric MDS that reconstructs a low-dimensional Euclidean representation from a given dissimilarity matrix. CMDS is effective when the given pairwise dissimilarities are precisely equal to the Euclidean distances and when the optimal low-dimensional configuration is accurately specified ([Oh and Raftery, 2001](#)). While CMDS is computationally efficient and widely used, its performance is limited when these assumptions do not hold. In many practical applications, dissimilarities may contain noise or measurement errors, leading to distortions in the recovered configuration. In such cases, alternative approaches, such as non-metric MDS or Bayesian formulations, may provide more robust solutions.

[Oh and Raftery \(2001\)](#) introduced a Bayesian multidimensional scaling (BMDS) approach that models observed dissimilarities as noisy observations of underlying Euclidean distances, incorporating measurement errors explicitly within a probabilistic model. Object locations in the low-dimensional space are estimated using Markov chain Monte Carlo (MCMC) sampling. Their results indicate that BMDS provides more accurate embeddings than CMDS, particularly when dissimilarities contain substantial measurement errors, the Euclidean assumption is violated, or the latent dimension is misspecified.

The Bayesian approach to the MDS problem has gained increasing attention due to its ability to incorporate prior information and handle measurement uncertainty. Several extensions of BMDS have been proposed to enhance its applicability. [Oh and Raftery \(2007\)](#) integrated Bayesian model-based clustering within the BMDS framework in [Oh and Raftery \(2001\)](#) to facilitate clustering in high-dimensional spaces. [Bakker and Poole \(2013\)](#) modeled observed distances using a log-normal distribution and estimated posteriors via squared error loss minimization. [Lin and Fong \(2019\)](#) employed a t -distribution for object locations, improving robustness against outliers and enabling variable selection through a latent multivariate regression structure. [Liu et al. \(2024\)](#) extended BMDS to hyperbolic manifolds, where dissimilarities are modeled as hyperbolic distances. Advancements in sampling methods have further improved the efficiency of BMDS. [Gronau and Lee \(2020\)](#) introduced differential evolution MCMC to enhance sampling performance, particularly in the context of psychologically interpretable metrics such as Euclidean and Minkowski distances. [Holbrook et al. \(2020\)](#) leveraged Hamiltonian Monte Carlo (HMC) ([Neal et al., 2011](#)) and massive parallelization using multi-core CPUs and GPUs to accelerate inference in BMDS, with applications in phylogenetics. Despite these

developments, a comprehensive Bayesian framework that accommodates non-Gaussian errors and extends beyond Euclidean spaces remains an open challenge. Moreover, while MCMC-based inference is widely used, its computational limitations motivate the exploration of alternative methods, such as sequential Monte Carlo (SMC), to improve scalability and efficiency.

Sequential Monte Carlo (SMC) methods have become an important alternative method for conducting Bayesian inference (see [Doucet et al., 2001](#); [Doucet and Johansen, 2009](#); [Chopin and Papaspiliopoulos, 2020](#), for an introduction to SMC). In general, SMC employs a population of weighted particles that evolve sequentially, allowing for greater parallelization and adaptability. SMC methods approximate a sequence of probability distributions using importance sampling and resampling mechanisms, yielding a flexible framework for unbiased estimation of marginal likelihoods ([Doucet et al., 2006](#)). A particularly relevant variant of SMC is the SMC sampler ([Del Moral et al., 2006](#); [Dai et al., 2022](#)), also known as annealed SMC (ASMC) ([Wang et al., 2021](#)). ASMC leverages an annealing schedule, similar to simulated tempering, to smoothly transition from an easy-to-sample distribution to the target posterior. This gradual adaptation reduces the risk of getting trapped in local modes and improves exploration of complex posterior landscapes under the same computational budget as standard MCMC. Notably, ASMC yields unbiased marginal likelihood estimators when using a fixed sequence of annealing parameters and nearly unbiased estimators when employing an adaptive annealing scheme. The estimated marginal likelihood enables robust Bayesian model comparison via Bayes factors ([Jeffreys, 1935](#); [Han and Carlin, 2001](#); [Zhou et al., 2016](#); [Wang et al., 2020](#)). The efficiency of ASMC has been demonstrated in diverse applications, including epidemiology ([Del Moral et al., 2012](#)), phylogenetics ([Wang et al., 2020](#)), and solving nonlinear differential equation systems ([Wang et al., 2021](#)). For a comprehensive review of recent advances in ASMC, see [Dai et al. \(2022\)](#).

The existing BMDS methods have several limitations. First, most BMDS methods assume Euclidean distance as the primary dissimilarity metric. However, Euclidean distance may not be suitable for certain applications. In medical imaging and 3D face recognition, surface alignment and shape comparison often rely on the Gromov-Hausdorff distance ([Mémoli, 2011](#)) or the partial embedding distance ([Bronstein et al., 2006](#)), which capture geometric distortions more effectively than Euclidean metrics. In text mining, Cosine dissimilarity ([Li and Han, 2013](#)) is preferred, as it measures the angle between document vectors and remains invariant to document length. Similarly, Jaccard dissimilarity ([Jaccard, 1901](#)) is widely used for set-based comparisons, particularly in short-text clustering. The lack of BMDS frameworks accommodating these alternative dissimilarities limits its applicability across diverse fields. Second, existing BMDS methods predominantly assume Gaussian noise in the observed dissimilarities, resulting in a lack of robustness and generality. Real-world datasets often exhibit heavy-tailed or skewed error distributions, leading to biased or inefficient estimates when using Gaussian-based models. Developing BMDS methods that incorporate more flexible error structures, such as Student's t -distributed errors or nonparametric approaches, remains an open problem. Third, research on model comparison within the BMDS framework remains scarce, particularly concerning the impact of different dissimilarity distributions. Most existing work focuses on comparing Bayesian and frequentist MDS solutions in

specific application domains. A systematic evaluation of BMDS models incorporating diverse dissimilarity metrics and error structures would provide deeper insights into their relative performance. Fourth, the increasing availability of high-dimensional data presents computational challenges for BMDS. Bayesian inference, while offering flexibility and uncertainty quantification, is often computationally expensive. Scaling BMDS methods to handle large datasets efficiently remains a critical issue, necessitating advances in inference techniques such as variational approximations, parallelized MCMC, or SMC methods.

To address key limitations in existing BMDS methods, such as reliance on Euclidean metrics, Gaussian error assumptions, and computational inefficiencies, we propose a generalized Bayesian multidimensional scaling (GBMDS) framework. GBMDS extends BMDS by incorporating flexible dissimilarity metrics and non-Gaussian error structures, enhancing robustness and applicability. We design an adaptive inference framework based on the annealed SMC algorithm to obtain Bayesian inference for the proposed GBMDS model. Unlike standard SMC methods that require designing novel proposal distributions, our approach leverages existing Metropolis-Hastings proposals. This facilitates seamless integration with established MCMC methodologies, reducing implementation complexity. Our adaptive annealed SMC algorithm is designed to handle dynamically increasing data, parameter dimensionality, and hidden variables. It enables adaptive inference to allow real-time updates as new data become available. This framework enables practitioners to update and refine posterior estimates incrementally as new data arrive, making it particularly suited for streaming or large-scale datasets. To enhance scalability, the proposed adaptive scheme processes large datasets in smaller batches, enabling efficient sequential Bayesian updates while mitigating computational bottlenecks.

Our contributions can be summarized as follows: (i) We generalize BMDS to accommodate non-Gaussian errors in the pairwise dissimilarities. This allows our model to handle data with heavy-tailed or skewed distributions, improving robustness and accuracy. (ii) Unlike conventional BMDS models restricted to Euclidean distances, GBMDS supports a broad class of dissimilarity measures, making it applicable to diverse domains, such as text mining. (iii) We introduce an efficient adaptive Bayesian inference framework based on annealed SMC. This approach mitigates computational burdens in large-scale applications while leveraging existing Metropolis-Hastings proposals, ensuring ease of implementation. (iv) Our framework provides nearly unbiased estimators of marginal likelihoods as a byproduct of sampling, which facilitates model selection through Bayes factors. This enables rigorous comparison between competing BMDS models with different error structures, dissimilarity metrics, and dimensions. (v) We evaluate the proposed GBMDS framework in three simulation studies and four real-world applications, demonstrating superior estimation accuracy and robustness across diverse dissimilarity metrics compared to benchmark methods.

The rest of this article is organized as follows. Section 2 describes the models for BMDS, including our proposed GBMDS model, specifications, model comparison, and identifiability considerations (Section 2.1–2.4). Section 3 depicts the implementation for the GBMDS model: Sections 3.1 and 3.2 detail the initialization and inference procedure,

while Section 3.3 outlines the adaptive mechanism with the annealed SMC algorithm. Simulations and real-world examples are presented in Sections 4 and 5. Finally, the conclusion and discussion are provided in Section 6.

2 BMDS Models

Suppose we have a set of n objects in the study. Let $\mathbf{Z} = \{\mathbf{z}_1, \dots, \mathbf{z}_n\}$ be a set of observed points with $\mathbf{z}_i = (z_{i,1}, \dots, z_{i,q})^\top \in \mathbb{R}^q$ representing the values of q attributes in object i . The value of q is usually high, which makes the visualization of the points in their original dimension hard. Let \mathbf{D} be the matrix of dissimilarities with entry $d_{i,j}$ as the dissimilarity between objects i and j . The dissimilarity matrix \mathbf{D} is computed from the observed data $\mathbf{z}_1, \dots, \mathbf{z}_n$ with specific dissimilarity metrics such as the Euclidean metric. Dissimilarity metrics used in this study will be detailed in Section 2.1. A formal definition of the metric space is given in *Supplementary*.

Let $\mathbf{x}_i = (x_{i,1}, \dots, x_{i,p})^\top \in \mathbb{R}^p$ be the unobserved vector representing the values of p significant attributes in object i . The goal of MDS methods is to find the set of points $\mathbf{X} = \{\mathbf{x}_1, \dots, \mathbf{x}_n\}$ such that $d_{i,j}$ and $\|\mathbf{x}_i - \mathbf{x}_j\|_p$ are as close as possible, where $\|\cdot\|_p$ represents the L^p norm. In such a manner, the given dissimilarities are well-reproduced by the resulting configuration. We refer to this process as object configuration (Oh and Raftery, 2001), which describes the estimation of values for objects' significant attributes.

CMDS is a commonly used dimension reduction technique for metric MDS developed by Torgerson (1952). CMDS assumes the dissimilarity to be Euclidean and takes the pairwise dissimilarities as inputs and outputs the coordinates of points in a low-dimensional space up to locations, rotations and reflections. Numerical optimization techniques can be used to find a solution to the minimization problem below:

$$\min \sum_{\substack{i,j=1 \\ i \neq j}}^n (d_{i,j} - \|\mathbf{x}_i - \mathbf{x}_j\|_p)^2. \quad (1)$$

The minimizers can be expressed analytically in terms of matrix eigendecompositions when the input dissimilarities satisfy the metric inequality and can be represented by Euclidean distances. CMDS can retrieve the complete configuration of objects (up to location shift) when the dissimilarities are precisely equal to the distances in the low-dimensional space and the dimension is appropriately specified. However, the dissimilarities between observed points are usually contaminated by errors, and the underlying dimensions are often unknown.

2.1 Generalized Bayesian multidimensional scaling

While Euclidean distance is one of the most widely used distance measures, it is not scale-invariant, meaning that distances computed from features might be skewed depending on the units. Moreover, Euclidean distance becomes less useful as the dimensionality of the data increases. To satisfy the various needs of different tasks, we develop

a general framework that can accommodate different distance metrics and behave robustly when outliers are present in the dissimilarities.

We restrict the dissimilarity measure $d_{i,j}$ to be strictly positive and assume that it follows a truncated distribution:

$$d_{i,j} \sim g(\delta_{i,j}) I(d_{i,j} > 0), \quad i \neq j, i, j = 1, \dots, n, \quad (2)$$

where $I(\cdot)$ is an indicator function. The true dissimilarity measure $\delta_{i,j}$ is modeled as the distance between object i and j using the dissimilarity metric \mathcal{D} :

$$\delta_{i,j} = \mathcal{D}(\mathbf{x}_i, \mathbf{x}_j). \quad (3)$$

The GBMDS framework we propose is general in nature. The various GBMDS models differ from one another based on the choice of dissimilarity metric \mathcal{D} and distribution function g .

Compared with the BMDS framework proposed in [Oh and Raftery \(2001\)](#), we do not restrict $d_{i,j}$ to be accompanied by Gaussian errors. The previous BMDS framework may be inadequate when dealing with dissimilarity measures that are subject to random errors or those that are non-Euclidean in nature. In addition, the assumption of utilizing a truncated Gaussian distribution to model the errors is inadequate in the presence of outliers. The presence of outliers can lead to increased uncertainty surrounding unobserved dissimilarities ($\delta_{i,j}$'s) beyond what can be accounted for by the tails of Gaussian distributions. We will refer to the framework in [Oh and Raftery \(2001\)](#) as the standard BMDS throughout this paper.

Dissimilarity metrics

The standard choice of dissimilarity metric \mathcal{D} on \mathbb{R}^p is the Euclidean metric (L^2 norm): $\mathcal{D}(\mathbf{x}_i, \mathbf{x}_j) = \|\mathbf{x}_i - \mathbf{x}_j\|_2 = \sqrt{\sum_{k=1}^p (x_{i,k} - x_{j,k})^2}$. It is often used in MDS when the dissimilarity matrix satisfies the metric axioms and has a well-defined Euclidean interpretation.

We generalize the standard BMDS by considering cases where the dissimilarity matrix may not have a well-defined Euclidean interpretation. In this case, we can consider candidate models with non-Euclidean dissimilarity metrics. For example, Cosine metric is defined as $\mathcal{D}(\mathbf{x}_i, \mathbf{x}_j) = 1 - (\sum_{k=1}^p x_{i,k} x_{j,k}) / \left(\sqrt{\sum_{k=1}^p x_{i,k}^2} \sqrt{\sum_{k=1}^p x_{j,k}^2} \right)$. This study utilizes the Cosine metric for text analysis using non-negative word frequencies, therefore, the Cosine metric of interest has a range from 0 to 1.

In our GBMDS framework, a variety of distributions can be considered for g , including both symmetric and skewed distributions. Symmetric distributions, such as Gaussian or Student's t -distributions, are suitable in some cases, while in other scenarios, a skewed distribution is more appropriate. In what follows, we will focus on the truncated skewed Gaussian distribution. This distribution is a suitable choice when the errors are skewed. Then, we will proceed to investigate the truncated Student's t -distribution. This distribution is deemed a suitable choice for robust estimation when outliers exist.

GBMDS with truncated skewed Gaussian distribution

We consider the possibility that some dissimilarities are both skewed and positive. We denote the model with truncated skewed Gaussian distribution as \mathcal{M}_{TSN} and model the dissimilarity $d_{i,j}$ as follows:

$$d_{i,j} | \mathcal{M}_{TSN} \sim \mathcal{TSN}(\delta_{i,j}, \sigma^2, \psi) I(0 < d_{i,j} < U), \quad i \neq j, i, j = 1, \dots, n,$$

where $\sigma^2 \in \mathbb{R}^+$ is the squared scale parameter, $\psi \in \mathbb{R}$ is the shape parameter, and U is the upper bound. The truncated Gaussian distribution is recovered when ψ is zero. As the absolute value of ψ grows, the absolute skewness of the distribution also increases, with negative ψ producing a left-skewed distribution and positive ψ generating a right-skewed distribution. Generally, the upper bound U for the truncated skewed Gaussian distribution can be set to infinity. However, for certain non-Euclidean dissimilarity metrics, it is necessary to impose an upper bound on $d_{i,j}$ to constrain the dissimilarities within a specific range. For example, when using the Cosine metric for text data, which ranges from 0 to 1, a natural choice for the upper bound is $U = 1$.

For a given matrix of dissimilarities \mathbf{D} , the likelihood function, l , of the latent variables $\mathbf{X} = \{\mathbf{x}_1, \dots, \mathbf{x}_n\}$, unknown parameters σ^2, ψ and U under \mathcal{M}_{TSN} , can be written as:

$$\begin{aligned} l(\mathbf{D} | \mathbf{X}, \sigma^2, \psi, U, \mathcal{M}_{TSN}) &\propto (\sigma^2)^{-\frac{m}{2}} \prod_{\substack{i,j=1 \\ i>j}}^n \{F_{\delta_{i,j}, \sigma, \psi}(U) - F_{\delta_{i,j}, \sigma, \psi}(0)\}^{-1} \\ &\times \exp \left\{ -\frac{1}{2\sigma^2} SSR \right\} \times \prod_{\substack{i,j=1 \\ i>j}}^n \Phi \left(\psi \frac{d_{i,j} - \delta_{i,j}}{\sigma} \right), \end{aligned} \quad (4)$$

where $F_{\delta_{i,j}, \sigma, \psi}(\cdot)$ is the cdf of skewed Gaussian distribution with location $\delta_{i,j}$, scale σ , and shape ψ , $SSR = \sum_{i>j} (d_{i,j} - \delta_{i,j})^2$ is the sum of squared residuals, $\Phi(\cdot)$ is the standard Gaussian cdf, and $m = n(n-1)/2$ is the total number of dissimilarities for n objects.

GBMDS with truncated Student's *t*-distribution

To further relax the assumption of constant Gaussian error variance in the dissimilarity, we introduce the model with truncated Student's *t*-distribution. Consequently, we can accommodate different degrees of uncertainty associated with dissimilarity by using different error variances. The *t*-distribution is often used as an alternative to the Gaussian distribution as a more robust model to fit data with heavier tails (Lange et al., 1989; Lin and Fong, 2019). In many applications, the outliers add more uncertainty around the tails of the dissimilarity measures. Fitting the truncated *t*-distribution provides a longer tail.

The *t*-distribution can be written in the form of its scale mixtures of Gaussian

representation to demonstrate its robustness property:

$$t_\nu(x; \mu, \sigma^2) = \int_0^\infty \mathcal{N}\left(x; \mu, \frac{\sigma^2}{\zeta}\right) \text{Gamma}\left(\zeta, \frac{\nu}{2}, \frac{\nu}{2}\right) d\zeta. \quad (5)$$

Equation (5) indicates that if a random variable x follows a t -distribution with mean μ , variance σ^2 , and degrees of freedom ν , then conditioning on $\zeta \sim \text{Gamma}(\nu/2, \nu/2)$, x follows a Gaussian distribution with parameters μ and σ^2/ζ . The t -distribution down-weights the observations which are disparate from the majority under the Gaussian distribution. This means that observations that are outliers or significantly different from the majority of the data will have less influence on the overall distribution in the t -distribution compared to the Gaussian distribution.

We denote the model with truncated t -distribution as \mathcal{M}_{TT} . \mathcal{M}_{TT} models the dissimilarity $d_{i,j}$ as follows:

$$\begin{aligned} \zeta_{i,j} &\sim \text{Gamma}(\nu/2, \nu/2), \\ d_{i,j} | \mathcal{M}_{TT} &\sim \mathcal{N}\left(\delta_{i,j}, \sigma^2/\zeta_{i,j}\right) I(0 < d_{i,j} < U), \quad i \neq j, i, j = 1, \dots, n. \end{aligned}$$

For a given matrix of dissimilarities \mathbf{D} , the likelihood function of the latent variables $\mathbf{X} = \{\mathbf{x}_1, \dots, \mathbf{x}_n\}$, unknown parameters σ^2 , $\zeta_{i,j}$ and U under \mathcal{M}_{TT} , can be written as:

$$\begin{aligned} l\left(\mathbf{D} | \mathbf{X}, \sigma^2, \zeta_{i,j}, U, \mathcal{M}_{TT}\right) &\propto \left(\sigma^2\right)^{-\frac{m}{2}} \times \\ &\exp \left\{ \frac{1}{2} \sum_{\substack{i,j=1 \\ i>j}}^n \log(\zeta_{i,j}) - \frac{1}{2\sigma^2} \sum_{\substack{i,j=1 \\ i>j}}^n \zeta_{i,j} (d_{i,j} - \delta_{i,j})^2 \right. \\ &\left. - \sum_{\substack{i,j=1 \\ i>j}}^n \log \left(\Phi\left(\frac{(U - \delta_{i,j}) \sqrt{\zeta_{i,j}}}{\sigma}\right) - \Phi\left(-\frac{\delta_{i,j} \sqrt{\zeta_{i,j}}}{\sigma}\right) \right) \right\}, \end{aligned} \quad (6)$$

where $\Phi(\cdot)$ and $m = n(n-1)/2$ are defined as in the model \mathcal{M}_{TSN} .

2.2 Bayesian inference

Prior distributions

Under the Bayesian framework, the prior distributions for the unknown parameters need to be specified in advance. We first introduce the prior distributions for model \mathcal{M}_{TSN} with unknown parameters \mathbf{x}_i , σ^2 , and ψ . We assume prior independence among parameters. For the prior of \mathbf{x}_i , we choose a multivariate Gaussian distribution with mean $\mathbf{0}$ and a diagonal covariance matrix $\Lambda = \text{diag}(\lambda_1, \dots, \lambda_p)$. In other words, $\mathbf{x}_i \sim \mathcal{N}(\mathbf{0}, \Lambda)$,

independently for $i = 1, \dots, n$. For the elements along the diagonal covariance matrix, we assume an inverse Gamma distribution for the hyperprior distribution, i.e., $\lambda_k \sim \mathcal{IG}(\alpha, \beta_k)$, independently for $k = 1, \dots, p$. Under this assumption, we posit independence among the latent variables, resulting in a simpler model with reduced hyperparameters and improved interpretability. For σ^2 , we use an inverse Gamma distribution for the prior distribution, i.e., $\sigma^2 \sim \mathcal{IG}(a, b)$. For ψ , we choose a diffuse prior, i.e., $\psi \sim \mathcal{U}(c, d)$. We denote the prior distributions of the unknown parameters as $\pi(\mathbf{X}|\Lambda)$, $\pi(\sigma^2)$, $\pi(\psi)$ and $\pi(\Lambda)$.

Next, we specify the prior distributions for model \mathcal{M}_{TT} with unknown parameters \mathbf{x}_i , σ^2 , and $\zeta_{i,j}$. We use the same settings for the prior distributions of \mathbf{x}_i and σ^2 as in model \mathcal{M}_{TSN} . In addition, we use $Gamma(\nu/2, \nu/2)$ as the prior distribution for $\zeta_{i,j}$.

Posterior distributions

For simplicity, we introduce a new notation \mathbf{s} to represent all the latent variables \mathbf{X} and the unknown parameters $\boldsymbol{\theta}$. Note that the parameters $\boldsymbol{\theta}$ vary across different models. In the model with truncated skewed Gaussian distribution, $\boldsymbol{\theta}$ includes σ^2 , ψ , and Λ . In the model with truncated Student's t -distribution, $\boldsymbol{\theta}$ includes σ^2 , ζ , and Λ .

In the Bayesian framework, our interest is the posterior distribution on \mathbf{s} given dissimilarity matrix \mathbf{D} , denoted as:

$$\pi(\mathbf{s}|\mathbf{D}) = \frac{\gamma(\mathbf{s}|\mathbf{D})}{M} \propto l(\mathbf{D}|\mathbf{s}) \times \pi(\mathbf{s}), \quad (7)$$

where $\gamma(\mathbf{s}|\mathbf{D})$ denotes the unnormalized posterior distribution, $l(\mathbf{D}|\mathbf{s})$ is the likelihood function, $\pi(\mathbf{s})$ is the prior on the parameters, and $M = \int \gamma(\mathbf{s}|\mathbf{D})d\mathbf{s}$ is the marginal likelihood. The likelihood functions are specified in Equations 4 and 6 for \mathcal{M}_{TSN} and \mathcal{M}_{TT} , respectively. The prior distributions are described in the previous subsection. Since the normalizing constant M is intractable, we will use Monte Carlo methods to approximate the posterior distributions, which will be detailed in Section 3.

Adaptive Bayesian inference

We propose an adaptive Bayesian inference framework for two key scenarios. First, in online inference, we sequentially update posterior estimates as new data arrive to allow for real-time updates. This approach is particularly useful when results need to be refined incrementally rather than recomputed from scratch. The main idea is to use the posterior distribution from a previous iteration to initialize the next. Second, for large datasets, instead of processing all observations at once, we can partition the data into smaller batches and perform inference sequentially. In BMDS, such an approach is especially beneficial as it enables dynamic visualization updates while managing computational efficiency. Here, we provide an overview of the adaptive Bayesian inference process. A detailed explanation of the adaptive mechanism is presented in Section 3.3.

Let $\mathbf{X}^{(0)}$ be the hidden variables associated with objects $\mathbf{Z}^{(0)} = \{\mathbf{z}_1, \dots, \mathbf{z}_{n_0}\}$, and $\mathbf{X}^{(1)}$ be the hidden variables associated with objects $\mathbf{Z}^{(1)} = \{\mathbf{z}_{n_0+1}, \dots, \mathbf{z}_{n_0+n_1}\}$. Here,

n_0 refers to the dimension of the original observations, and n_1 refers to the incremental dimension of the additional observations. Given dissimilarity metric \mathcal{D} , dissimilarities $\mathbf{D}^{(0)}$ is obtained from $\mathbf{Z}^{(0)}$ and \mathbf{D} is obtained from $\mathbf{Z} = (\mathbf{Z}^{(0)}, \mathbf{Z}^{(1)})$.

In this case, \mathbf{s} is composed of three parts, $\mathbf{X}^{(0)}$, $\mathbf{X}^{(1)}$, and $\boldsymbol{\theta}$. The posterior distribution of \mathbf{s} can be rewritten as:

$$\pi(\mathbf{X}^{(0)}, \mathbf{X}^{(1)}, \boldsymbol{\theta} | \mathbf{D}) \propto l(\mathbf{D} | \mathbf{X}^{(0)}, \mathbf{X}^{(1)}, \boldsymbol{\theta}) \pi(\mathbf{X}^{(0)} | \Lambda^{(0)}) \pi(\mathbf{X}^{(1)} | \Lambda^{(1)}) \pi(\boldsymbol{\theta}). \quad (8)$$

The adaptive Bayesian inference concerns the inference of $\pi(\mathbf{X}^{(0)}, \mathbf{X}^{(1)}, \boldsymbol{\theta} | \mathbf{D})$ using the previous inference for $\pi(\mathbf{X}^{(0)}, \boldsymbol{\theta} | \mathbf{D}^{(0)})$ when dissimilarity data increase from $\mathbf{D}^{(0)}$ to \mathbf{D} .

When the previous dissimilarity matrix $\mathbf{D}^{(0)}$ is not available, we denote $\mathbf{D}^{(0)} = \emptyset$ and $\mathbf{X}^{(0)} = \emptyset$. With our notation, the posterior distribution in Equation 7 is a special case of Equation 8 when $\mathbf{D}^{(0)} = \emptyset$, $\mathbf{X}^{(0)} = \emptyset$. Therefore, we will only focus on the adaptive Bayesian inference with Monte Carlo methods for Equation 8 in Section 3.

2.3 Model comparison

As described in the previous section, the function g can take different forms. In most cases, the optimal form of g , the number of significant attributes p or the applied dissimilarity metrics are unknown. In this section, we approach the problem of comparing a discrete set of Bayesian models with the Bayes factor. Consider two models \mathcal{M}_1 and \mathcal{M}_2 with different likelihoods and corresponding sets of parameters \mathbf{s}_1 and \mathbf{s}_2 . In the context of this paper, \mathcal{M}_1 and \mathcal{M}_2 would correspond to two competing models. Examples of competing models could be \mathcal{M}_{TSN} versus \mathcal{M}_{TT} , or one model under a different choice of dimension p . The Bayes factor is defined as the ratio of the posterior odds to the prior odds. When the two models have equal prior probability, the Bayes Factor reduces to the ratio of two marginal likelihood estimates, and is given by:

$$\text{Bayes Factor}(\mathcal{M}_1, \mathcal{M}_2) = \frac{\int \pi(\mathbf{s}_1 | \mathcal{M}_1) l(\mathbf{D} | \mathbf{s}_1, \mathcal{M}_1) d\mathbf{s}_1}{\int \pi(\mathbf{s}_2 | \mathcal{M}_2) l(\mathbf{D} | \mathbf{s}_2, \mathcal{M}_2) d\mathbf{s}_2} = \frac{P(\mathbf{D} | \mathcal{M}_1)}{P(\mathbf{D} | \mathcal{M}_2)}.$$

Bayes factor can provide support to either model; a Bayes factor greater than 1 indicates support for model 1 over model 2 and vice versa. A rule of thumb, as suggested in [Kass and Raftery \(1995\)](#), can be viewed as guidelines for model selection from a Bayes factor. According to these guidelines, a Bayes factor falling within the range of 1 to 3 shows weak evidence, while a Bayes factor spanning from 3 to 10 implies substantial evidence. A Bayes factor exceeding 10 is considered as strong evidence. A typical challenge for using the Bayes factor is the computation of the marginal likelihood estimates, especially for MCMC-based methods ([Wang et al., 2020](#)). Marginal likelihood estimation is not straightforward in MCMC-based methods, and additional sampling procedures are needed to obtain these estimates. Several methods have been proposed to address this issue ([Chib and Jeliazkov, 2001](#); [Skilling, 2004](#); [Robert and Wraith, 2009](#)), but each has its drawbacks. One additional limitation shared by all MCMC-based marginal likelihood estimators is that they are generally biased. In contrast, SMC naturally produces

unbiased or nearly unbiased marginal likelihood estimators as a byproduct of sampling, enabling straightforward model comparison via the Bayes factor.

On the other side, in the frequentist view, STRESS is a commonly used measure of fit for the object configuration problem (Kruskal, 1964). STRESS value is defined as

$$\text{STRESS} = \sqrt{\frac{\sum_{i>j} (d_{i,j} - \hat{d}_{i,j})^2}{\sum_{i>j} d_{i,j}^2}}, \quad i, j = 1, \dots, n,$$

where $\hat{d}_{i,j}$ is the distance found from the estimated object configuration. MDS methods form an object configuration that minimizes the STRESS values. A smaller STRESS value indicates a better fit.

In this work, we will select the optimal Bayesian model and dimension p using the marginal likelihood estimates. We will compare and evaluate the performances of CMDS and GBMDS using the STRESS value.

2.4 Identifiability in multidimensional scaling

Similar to other dimensional reduction methods, identification issues arise in the posterior inference of GBMDS. For instance, the center and direction of the estimated points can be arbitrary. To address this, we standardize all posterior samples of \mathbf{x}_i 's using Procrustes transformations (Goodall, 1991). This method aligns configurations using a least-squares criterion by a combination of scaling, rotation, reflection, and translation. After the Procrustes transformation, we construct credible regions from the adjusted posterior samples of \mathbf{x}_i to quantify uncertainty.

3 Adaptive Bayesian Inference using Annealed SMC

3.1 Intermediate distributions and particle initialization

To conduct the Bayesian inference for the posterior distribution in Equation 8, we propose to design an artificial sequence of annealing intermediate target distributions following the ideas from the SMC literature (Neal, 2001; Del Moral et al., 2006, 2007; Wang et al., 2020). Specifically, we create a sequence of annealing intermediate target distributions $\{\pi_r(\mathbf{s})\}_{0 \leq r \leq R}$, such that

$$\pi_r(\mathbf{s}) \propto \gamma_r(\mathbf{s}) = \left(l(\mathbf{D}|\mathbf{s}) \pi(\mathbf{s}) \right)^{\tau_r} \times \tilde{\pi}_0(\mathbf{s})^{1-\tau_r}, \quad (9)$$

where $\tilde{\pi}_0(\mathbf{s})$ is a *reference distribution* that is generally easy to sample from (Fan et al., 2011), and $0 = \tau_0 < \tau_1 < \dots < \tau_R = 1$ is a sequence of annealing parameters. If τ_r is zero, the distribution becomes the reference distribution $\tilde{\pi}_0(\mathbf{s})$. At the other extreme, the distribution is the posterior distribution of interest when the power τ_r equals 1.

In our model, \mathbf{s} is a vector of all the variables in $\mathbf{X}^{(0)}$, $\mathbf{X}^{(1)}$, and $\boldsymbol{\theta}$. The reference distribution can be specified for $\mathbf{X}^{(0)}$, $\mathbf{X}^{(1)}$ and $\boldsymbol{\theta}$ independently:

$$\tilde{\pi}_0(\mathbf{s}) = \tilde{\pi}_0(\mathbf{X}^{(0)}) \tilde{\pi}_1(\mathbf{X}^{(1)}) \tilde{\pi}_0(\boldsymbol{\theta}). \quad (10)$$

Preferably, the reference distributions should possess properties that allow for convenient sampling and proximity to the modes of the target distribution. For simplicity, we choose the reference distribution for $\boldsymbol{\theta}$ to be its prior distribution, i.e. $\tilde{\pi}_0(\boldsymbol{\theta}) = \pi(\boldsymbol{\theta})$, and the reference distributions for $\mathbf{X}^{(1)}$ to be its prior, $\tilde{\pi}_1(\mathbf{X}^{(1)}) = \pi(\mathbf{X}^{(1)}|\Lambda^{(1)})$; the reference distributions for $\mathbf{X}^{(0)}$, denoted $\tilde{\pi}_0(\mathbf{X}^{(0)})$, is set to be a Gaussian distribution.

With a small value of τ_r , the intermediate target distribution is closer to the reference distribution. For parameters that rely on the prior distribution as the reference distribution, smaller τ_r can result in flatter intermediate target distributions that facilitate the movement between various modes. The samples are coerced into the posterior distribution as we slowly increase the annealing parameter τ_r . The initialization of particles is summarized in Algorithm 1.

Algorithm 1: Particle_Initialization

Input : (a) Dissimilarity: $\mathbf{D}^{(0)}, \mathbf{D}$; (b) Priors and reference distributions over $\{\mathbf{x}_1, \dots, \mathbf{x}_n\}$ and model parameters $\boldsymbol{\theta} = \{\sigma^2, \Lambda, \psi, \zeta\}$; (c) Number of particles: K .

Output: Initializations of K particles: $\{\mathbf{s}_{0,k}\}_{k=1}^K$.

```

1 for  $k \in \{1, 2, \dots, K\}$  do
2   if  $\mathbf{D}^{(0)} \neq \emptyset$  then
3      $\quad$  Initialize particles of  $\mathbf{X}_{0,k}^{(0)} \sim \tilde{\pi}_0(\mathbf{X}^{(0)})$ .
4     Initialize particles of  $\mathbf{X}_{0,k}^{(1)} \sim \tilde{\pi}_1(\mathbf{X}^{(1)})$ .
5     Initialize particles of parameters with independent samples from prior distributions:
        $\{\sigma_{0,k}^2, \Lambda_{0,k}, \psi_{0,k}, \zeta_{0,k}\} \sim \pi(\boldsymbol{\theta})$ .

```

3.2 Annealed SMC

This section will consider the annealed SMC algorithm for a fixed dimension where the previous dissimilarity matrix $\mathbf{D}^{(0)}$ is unavailable. We will introduce in Algorithm 2 the annealed SMC algorithm along with the adaptive mechanism for choosing the annealing sequence. The annealed SMC algorithm approximates the posterior distribution $\pi(\mathbf{s}|\mathbf{D})$ in R steps. At each step r , we approximate $\pi_r(\cdot)$ using a total of K particles. Each particle $\mathbf{s}_{r,k}$ is associated with a positive weight. Let $w_{r,k}$ denote the unnormalized weight for particle $\mathbf{s}_{r,k}$ and let $W_{r,k}$ denote the corresponding normalized weight. The normalization is performed by $W_{r,k} = w_{r,k} / \sum_{k=1}^K w_{r,k}$.

We start by sampling initial particles from the reference distributions. Then, the annealed SMC algorithm iterates between *reweighting*, *propagating*, and *resampling*. The details of the three steps in the annealed SMC algorithm are given as follows.

Step 1. Weight Update

The incremental importance weight for particle k at iteration r is

$$\tilde{w}_{r,k} = \frac{\gamma_r(\mathbf{s}_{r,k}) \times \kappa^-(\mathbf{s}_{r,k}, \mathbf{s}_{r-1,k})}{\gamma_{r-1}(\mathbf{s}_{r-1,k}) \times \kappa^+(\mathbf{s}_{r-1,k}, \mathbf{s}_{r,k})}, \quad (11)$$

where the forward kernel $\kappa^+(\mathbf{s}_{r-1,k}, \mathbf{s}_{r,k})$ is a π_r -invariant Metropolis-Hastings kernel, and $\kappa^-(\mathbf{s}_{r,k}, \mathbf{s}_{r-1,k})$ is the backward kernel (Del Moral et al., 2006). The selection of the backward kernel is crucial as it will affect the variance of the normalized weights. A convenient backward kernel that allows easy computation of the weight is

$$\kappa^-(\mathbf{s}_{r,k}, \mathbf{s}_{r-1,k}) = \frac{\gamma_r(\mathbf{s}_{r-1,k}) \times \kappa^+(\mathbf{s}_{r-1,k}, \mathbf{s}_{r,k})}{\gamma_r(\mathbf{s}_{r,k})}. \quad (12)$$

This approach simplifies the evaluation of weights since we do not need point-wise evaluations of the backward and forward kernels. The incremental importance weight becomes

$$\tilde{w}_{r,k} = \left[\frac{l(\mathbf{D}|\mathbf{s}_{r-1,k}) \pi(\mathbf{s}_{r-1,k})}{\tilde{\pi}_0(\mathbf{s}_{r-1,k})} \right]^{\tau_r - \tau_{r-1}}. \quad (13)$$

The weight update function for particles at iteration r is

$$W_{r,k} \propto w_{r,k} = w_{r-1,k} \tilde{w}_{r,k}.$$

Note the weight update function only depends on the particles at the previous iteration. This is implemented in Line 9 of Algorithm 2.

Step 2. Particle Propagation

We sample the new particles $\mathbf{s}_{r,k}$ from π_r -invariant Metropolis-Hastings kernels. At each step r , we have the option to sample either all parameters or a subset of the parameters, depending on the desired trade-off between computational efficiency and effective exploration of the parameter space. In particular, for a high-dimensional parameter $\{\mathbf{x}_1, \dots, \mathbf{x}_n\}$, updating a subset of it can help mitigate the risk of low acceptance rates. This approach allows for more targeted exploration of the parameter space and potentially results in faster mixing. The annealed SMC algorithm can directly make use of the MCMC proposals in the particle propagation. The full conditional distributions for parameters λ_k , $\{\mathbf{x}_1, \dots, \mathbf{x}_n\}$, σ^2 , and $\zeta_{i,j}$ are presented below. In each conditional posterior distribution, we use $|\dots$ to denote conditioning on the data and all other parameters and/or indicators. A detailed description of sampling methods is given in *Supplementary*.

The full conditional distribution for λ_k is

$$\lambda_k | \dots \sim IG(\alpha + n/2, \beta_k + \tau_r v_k/2), \quad (14)$$

where v_k/n is the sample variance of the k th coordinates of \mathbf{x}_i 's.

The full conditional posterior distributions of $\{\mathbf{x}_1, \dots, \mathbf{x}_n\}$, σ^2 and ψ do not admit closed forms, a random walk Metropolis-Hastings step is implemented with the Gaussian proposal densities.

For \mathcal{M}_{TSN} ,

$$\begin{aligned}\gamma_r(\{\mathbf{x}_1, \dots, \mathbf{x}_n\} | \dots, \mathcal{M}_{TSN}) &\propto \exp \left\{ -\tau_r \left(A + \frac{1}{2} \sum_{i=1}^n \mathbf{x}_i^\top \Lambda^{-1} \mathbf{x}_i \right) \right\}, \\ \gamma_r(\sigma^2 | \dots, \mathcal{M}_{TSN}) &\propto \sigma^{-2(a+1)} \exp \left\{ -\tau_r \left(A + \frac{b}{\sigma^2} \right) \right\},\end{aligned}$$

where $A = \frac{1}{2\sigma^2} SSR + \frac{m}{2} \log \left(\sigma^2 (F_{\delta_{i,j}, \sigma, \psi}(U) - F_{\delta_{i,j}, \sigma, \psi}(0)) \right) - \sum_{i>j} \log \left(\Phi \left(\psi \frac{d_{i,j} - \delta_{i,j}}{\sigma} \right) \right)$.

For \mathcal{M}_{TT} ,

$$\begin{aligned}\gamma_r(\{\mathbf{x}_1, \dots, \mathbf{x}_n\} | \dots, \mathcal{M}_{TT}) &\propto \exp \left\{ -\tau_r \left(C + \frac{1}{2} \sum_{i=1}^n \mathbf{x}_i^\top \Lambda^{-1} \mathbf{x}_i \right) \right\}, \\ \gamma_r(\sigma^2 | \dots, \mathcal{M}_{TT}) &\propto \sigma^{-m} \exp \left\{ -\tau_r \left(C + \frac{b}{\sigma^2} \right) \right\},\end{aligned}$$

where $C = \frac{1}{2\sigma^2} \sum_{i>j} \zeta_{i,j} (d_{i,j} - \delta_{i,j})^2 + \sum_{i>j} \log \left(\Phi \left(\frac{(U - \delta_{i,j}) \sqrt{\zeta_{i,j}}}{\sigma} \right) - \Phi \left(-\frac{\delta_{i,j} \sqrt{\zeta_{i,j}}}{\sigma} \right) \right)$.

For model \mathcal{M}_{TT} , the full conditional distribution for $\zeta_{i,j}$ is

$$\zeta_{i,j} | \dots, \mathcal{M}_{TT} \sim \text{Gamma}((\tau_r + \nu)/2, \tau_r(d_{i,j} - \delta_{i,j})^2/(2\sigma^2) + \nu/4). \quad (15)$$

Step 3. Particle Resampling

To alleviate the issue that all normalized weights converge to 0 except for one particle in sequential importance sampling, we prune particles of low weights when the population becomes too unbalanced. Popular resampling schemes include, but are not limited to, multinomial resampling, systematic resampling, stratified resampling, and residual resampling (Douc and Cappé, 2005). We will use multinomial resampling, as it is the most commonly used resampling method in the SMC literature.

Resampling at each iteration will increase the variance of the importance weights. Therefore, the resampling step is performed only when the degeneracy of the particles reaches some threshold ϵ . At each iteration r , we monitor the degeneracy of particles using the effective sampling size (ESS) (Kong, 1992):

$$\text{ESS} = \frac{1}{\sum_{k=1}^K (W_{r,k})^2}. \quad (16)$$

Algorithm 2: Annealed_SMC

Input : (a) Initialization of K particles: $\{s_{0,k}\}_{k=1}^K$; (b) Priors and reference distributions over model parameters $\mathbf{s} = \{\{\mathbf{x}_1, \dots, \mathbf{x}_n\}, \sigma^2, \Lambda, \psi, \zeta\}$; (c) Likelihood function $l(\mathbf{D}|\mathbf{s})$; (d) rCESS threshold ϕ ; (e) Resampling threshold ϵ .

Output: (a) Particle population: $\{(s_{R,k}, W_{R,k})\}_{k=1}^K$; (b) Marginal likelihood estimates: \widehat{M}_R ; (c) Total SMC iterations: R ; (d) Sequence of annealing parameter: $\{\tau_r\}_{r=0}^R$.

1 Initialize SMC iteration index: $r \leftarrow 1$, initialize annealing parameter: $\tau_0 \leftarrow 0$, initialize marginal likelihood estimate: $\widehat{M}_0 \leftarrow 1$, load initial particles $\{s_{0,k}\}_{k=1}^K$.

2 **for** $k \in \{1, 2, \dots, K\}$ **do**

3 $w_{r,k} = 1$, $W_{r,k} = 1/K$.

4 **for** $r \in \{2, 3, \dots\}$ **do**

5 **for** $k \in \{1, 2, \dots, K\}$ **do**

6 Compute incremental importance weights: $\tilde{w}_{r,k} = \left[\frac{l(\mathbf{D}|s_{r-1,k})\pi(s_{r-1,k})}{\tilde{\pi}(s_{r-1,k})} \right]^{\tau - \tau_{r-1}}$.

7 Determine the next annealing parameter τ_r using bisection method with:
 $f(\tau) = \text{rCESS}_r(W_{r-1,\cdot}, w_{r,\cdot}) = \phi$.

8 **for** $k \in \{1, 2, \dots, K\}$ **do**

9 Compute pre-resampling unnormalized weights: $w_{r,k} = w_{r-1,k} \times \tilde{w}_{r,k}$.

10 Normalize weights: $W_{r,k} = w_{r,k} / (\sum_{k=1}^K w_{r,k})$.

11 Sample particles $s_{r,k}$ from π_{τ_r} -invariant Metropolis-Hastings kernels.

12 Update marginal likelihood estimates $\widehat{M}_r = \widehat{M}_{r-1} \times \sum_{k=1}^K W_{r-1,k} \tilde{w}_{r,k}$.

13 **if** $\tau_r = 1$ **then**

14 The total number of SMC iterations $R \leftarrow r$.

15 return R , $\{\tau_r\}_{r=0}^R$, $\{(s_{R,k}, W_{R,k})\}_{k=1}^K$, and \widehat{M}_R ,

16 **else**

17 **if** *particle degeneracy is too severe, i.e. $rESS < \epsilon$* **then**

18 Resample the particles, denoted $\{s_{r,k}\}_{k=1}^K$;

19 Reset particle weights: $w_{r,k} = 1$, $W_{r,k} = 1/K$.

The relative effective sample size (rESS) normalizes the ESS between zero and one. The rESS at iteration r can be calculated by $\text{rESS} = \text{ESS}/K$.

The annealed SMC algorithm produces a set of particles. After the extra resampling step in the end, the output of the annealed SMC algorithm contains a list of K particles with equal weight. These particles can be used for the posterior approximation and for constructing the visualization in the lower-dimensional space. To find the Bayesian estimate of \mathbf{X} , we take an approximate posterior mode of $\{\mathbf{x}_1, \dots, \mathbf{x}_n\}$ as described in [Oh and Raftery \(2001\)](#). [Oh and Raftery \(2001\)](#) observed that the term involving SSR dominates the posterior density. Thus, the approximate posterior mode can be found by the values of $\{\mathbf{x}_1, \dots, \mathbf{x}_n\}$ that minimizes SSR among all K particles. The approximate posterior mode retrieves the relative positions of $\{\mathbf{x}_1, \dots, \mathbf{x}_n\}$, and they can be considered as the solution to the object configuration. Meaningful absolute positions of \mathbf{X} may be obtained from some suitable transformation defined by the users if needed.

Some challenges arise with MCMC-based approximations in the context of model comparison via marginal likelihood estimators, as discussed in [2.3](#). MCMC-based algorithms often require additional computational costs to estimate the marginal likelihood separately. In contrast, model selection can be accomplished effortlessly using the Bayes factor in the proposed annealed SMC algorithm. When resampling is not performed at every step, the estimated marginal likelihood could be evaluated during the sampling process with the following formula:

$$\widehat{M}_R = \prod_{r=1}^R \sum_{k=1}^K W_{r-1,k} \tilde{w}_{r,k}.$$

Moreover, the estimates are unbiased when using a fixed annealing sequence and nearly unbiased with an adaptive annealing scheme. Previous studies have shown the advantages of SMC over MCMC for model comparison via marginal likelihood estimators ([Zhou et al., 2016](#); [Wang et al., 2020](#)).

The sequence of intermediate target distributions, as defined in [Equation 9](#), is determined by the choice of the annealing sequence, $\{\tau_r\}$. Proper selection of the sequence of annealing parameters is one challenge in the annealed SMC. A large number of annealing parameters can improve the performance, but increase the computational cost. In order to ensure the proposed particles from the current iteration can effectively approximate the subsequent intermediate target distribution, it is necessary to transition smoothly from the reference distribution ($\tau_0 = 0$) to the posterior distribution ($\tau_R = 1$).

We apply the adaptive annealing parameter scheme discussed in [Wang et al. \(2020\)](#). The main idea is to select an annealing parameter τ such that we achieve a controlled increase in particle degeneracy. The particle degeneracy between two successive intermediate distributions is measured by the relative conditional effective sample size (rCESS) ([Zhou et al., 2016](#)),

$$\text{rCESS}_r (W_{r-1,\cdot}, \tilde{w}_{r,\cdot}) = \frac{\left(\sum_{k=1}^K W_{r-1,k} \tilde{w}_{r,k} \right)^2}{\sum_{k=1}^K W_{r-1,k} (\tilde{w}_{r,k})^2}. \quad (17)$$

Values of rCESS range from $1/K$ to 1. With the $\tilde{w}_{r,k}$ in Equation 13, rCESS_r is a decreasing function of τ_r , where $\tau_r \in (\tau_{r-1}, 1]$. The value of rCESS over iterations is controlled by choosing the annealing parameter τ such that

$$f(\tau) = \text{rCESS}_r(W_{r-1, \cdot}, \tilde{w}_{r, \cdot}) = \phi, \quad (18)$$

where $\phi \in (0, 1)$ is a tuning parameter that controls the length of the sequence τ_r . Since there exists no closed-form solution for τ by solving $f(\tau) = \phi$, a bisection method is used to solve this one-dimensional search problem. The search interval is $\tau_r \in (\tau_{r-1}, 1]$. Given that f is a continuous function with $f(\tau_{r-1}) - \phi > 0$ and $f(1) - \phi < 0$ (otherwise set $\tau_r = 1$), it follows that there must exist an intermediate point τ^* with $f(\tau^*) = \phi$. This is implemented in Line 7 of Algorithm 2.

3.3 Adaptive mechanism

In the previous subsection, we presented the annealed SMC algorithm for a fixed dimension. In this section, we will describe an adaptive mechanism to enable the annealed SMC algorithm to handle increasing dimensions. The complete algorithm is presented in Algorithm 3.

Inferences are made sequentially for each batch of observations. When a new batch is available, the dissimilarity matrix $\mathbf{D} = \{\mathbf{D}^{(0)}, \mathbf{D}^{(1)}\}$ is calculated based on all the old observations and the incremental observations. The primary objective is to conduct inference for $\pi(\mathbf{X}^{(0)}, \mathbf{X}^{(1)}, \boldsymbol{\theta} | \mathbf{D})$. In order to achieve this objective, we employ the strategy detailed in Section 3.1 for initializing the particles of $\mathbf{s} = \{\mathbf{X}^{(0)}, \mathbf{X}^{(1)}, \boldsymbol{\theta}\}$.

When previous estimations are unavailable, i.e., $\mathbf{D}^{(0)} = \emptyset$, $\mathbf{X}^{(0)} = \emptyset$, the reference distribution for $\mathbf{X}^{(1)} = \{\mathbf{x}_1, \dots, \mathbf{x}_n\}$ is based on the results from fitting CMDS:

$$\mathbf{x}_i \sim \mathcal{N}(\mathbf{x}_i^{\text{CMDS}}, 0.01\mathbf{I}), \text{ independently for } i = 1, \dots, n,$$

where $\mathbf{x}_i^{\text{CMDS}}$ is the result from fitting CMDS on $\mathbf{D}^{(1)}$. The variance of the reference distribution is selected in a manner that induces the particles to concentrate around the CMDS outputs. With a small value of the annealing parameter τ_r , the intermediate target distribution is closer to the reference distribution, which is concentrated around the CMDS outputs for $\mathbf{D}^{(1)}$.

When $\mathbf{D}^{(0)} \neq \emptyset$ and $\mathbf{X}^{(0)} \neq \emptyset$, we choose the reference distribution to be a particle approximation to the posterior distribution of $\mathbf{X}^{(0)}$ given $\mathbf{D}^{(0)}$. The reference distribution for $\mathbf{X}^{(0)} = \{\mathbf{x}_1, \dots, \mathbf{x}_{n_0}\}$ is based on the results from all particles:

$$\mathbf{x}_i \sim \mathcal{N}(\hat{\mathbf{x}}_i, \hat{\boldsymbol{\Sigma}}), \text{ independently for } i = 1, \dots, n_0,$$

where $\hat{\mathbf{x}}_i$ is the particles' posterior mode and $\hat{\boldsymbol{\Sigma}}$ is the estimated covariance matrix of all observations' particles' posterior modes from the previous computation. For the new incremental set $\mathbf{X}^{(1)}$ in \mathbf{s} , we sample initial particles from the reference distribution, which is selected as its prior distribution for simplicity. This completes the specifications

of the reference distributions in Algorithm 1. Initialization of particles is implemented from Line 3 to Line 9 of Algorithm 3.

As an example, suppose we already obtain the posterior samples of $\mathbf{X}^{(0)}$ from n_0 old observations by running the annealed SMC algorithm, and an extra of n_1 new observations become available. In that case, instead of running the annealed SMC algorithm from scratch using $n = n_0 + n_1$ observations, we can utilize the information from the posterior samples of $\mathbf{X}^{(0)}$ to initialize values for the old observations and use the prior distribution to initialize samples for the new observations $\mathbf{X}^{(1)}$. One example that illustrates the case details with incremental dimensions is given in Section 5.1.

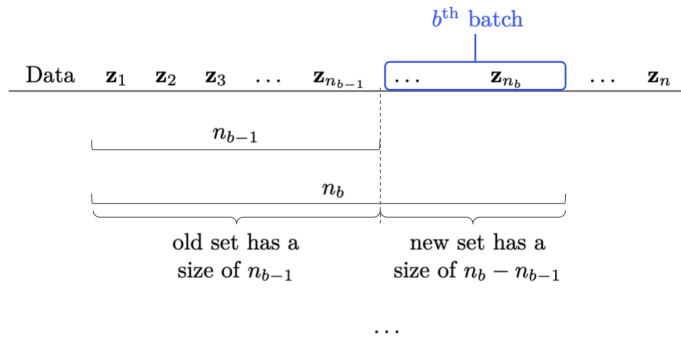


Figure 1: An illustration of the batch split.

In general, we can consider splitting data into B batches; each batch has a size of $n_b - n_{b-1}$, for $b = 1, \dots, B$, with $n_0 = 0$. Figure 1 illustrates the setup for the adaptive mechanism when b^{th} batch of data with size $n_b - n_{b-1}$ is observed after the posterior samples of n_{b-1} old observations are obtained. Each batch is proceeded sequentially as outlined in Algorithm 3.

4 Simulation Studies

The primary objective of the simulation studies is to evaluate the performance of various models under diverse data structures. We compared several candidate models, denoted as $\mathcal{M}_g^{\mathcal{D}}$, where g represents the model distribution for dissimilarities and \mathcal{D} is the dissimilarity metric used during estimation. We examined three experimental settings: one with known underlying dimensions, one with skewed errors, and the other with outliers. We also conducted a runtime analysis to compare the computation costs of various candidate models using both the proposed annealed SMC algorithm and the MCMC algorithm introduced in Oh and Raftery (2001). To maintain comparability between the two Bayesian methods, we kept a consistent computational budget. Initially, the annealed SMC was executed with K particles, and the number of iterations was recorded. Subsequently, we equitably allocated this computational budget to MCMC by setting the number of MCMC iterations equal to the product of the annealed SMC iterations

Algorithm 3: Adaptive_Annealed_SMC

Input : (a) Number of batches: B ; (b) Data: $\mathbf{Z} = \{\mathbf{z}_1, \dots, \mathbf{z}_n\}$; (c) Dissimilarity metric: \mathcal{D} .

Output: (a) Marginal likelihood estimates \widehat{M}_R ; (b) Posterior approximation,
 $\hat{\pi}(\mathbf{s}) = \sum_{k=1}^K W_{R,k} \times \delta_{\mathbf{s}_{R,k}}(\mathbf{s})$.

```

1 for  $b \in \{1, 2, \dots, B\}$  do
2   Calculate dissimilarities  $\mathbf{D}$  from  $\{\mathbf{z}_1, \dots, \mathbf{z}_{n_b}\}$  with a given dissimilarity metric  $\mathcal{D}$ .
3   if  $b = 1$  then
4     Set both  $\mathbf{D}^{(0)}$  and  $\tilde{\pi}_0(\cdot)$  to  $\emptyset$ .
5     Set  $\tilde{\pi}_1(\mathbf{x}_i)$  to  $\mathcal{N}(\mathbf{x}_i | \mathbf{x}_i^{\text{CMDS}}, 0.01\mathbf{I})$  for  $i = 1, \dots, n_1$ .
6   else
7     Set  $\tilde{\pi}_0(\mathbf{x}_i)$  to  $\mathcal{N}(\mathbf{x}_i | \hat{\mathbf{x}}_i, \hat{\Sigma})$  for  $i = 1, \dots, n_{b-1}$ .
8     Set  $\tilde{\pi}_1(\mathbf{x}_i)$  to  $\mathcal{N}(\mathbf{x}_i | \mathbf{0}, \Lambda)$  for  $i = n_{b-1} + 1, \dots, n_b$ .
9    $\{\mathbf{s}_{0,k}\}_{k=1}^K \leftarrow \text{Particle\_Initialization}(\mathbf{D}^{(0)}, \mathbf{D}, \tilde{\pi}_0(\mathbf{X}), \tilde{\pi}_1(\mathbf{X}), \pi(\theta), K)$ 
10   $\{(\mathbf{s}_{R,k}, W_{R,k})\}_{k=1}^K, \widehat{M}_R \leftarrow \text{Annealed\_SMC}(\{\mathbf{s}_{0,k}\}_{k=1}^K, \tilde{\pi}_0(\mathbf{X}), \tilde{\pi}_1(\mathbf{X}), \pi(\theta), l(\mathbf{D}|\mathbf{s}), \phi, \epsilon)$ 
11  Posterior approximation:  $\hat{\pi}(\mathbf{s}^{(b)}) = \sum_{k=1}^K W_{R,k} \times \delta_{\mathbf{s}_{R,k}}(\mathbf{s})$ .
12  Compute the weighted mean  $\hat{\mathbf{x}}_i$  and covariance  $\hat{\Sigma}$ ,  $i = 1, \dots, n_b$  from  $\{(\mathbf{s}_{R,k}, W_{R,k})\}_{k=1}^K$ .
13  Reset  $\mathbf{D}^{(0)} \leftarrow \mathbf{D}$ .

```

and the number of particles. For the implementation of the MCMC algorithm in [Oh and Raftery \(2001\)](#), we utilized the available R package BayMDS by [Oh and Lee \(2022\)](#), which implements the truncated Gaussian model.

We established the values for the prior parameters by utilizing empirical Bayes methods, following the recommendations outlined in [Oh and Raftery \(2001\)](#). For the prior of σ^2 , we chose $a = 5$ and $b = SSR/m$ obtained from CMDS. For the prior of ψ , we chose $c = -2$ and $d = 2$. For the hyperprior of λ_k , we set $\alpha = 1/2$ and $\beta_k = \frac{1}{2}v_k^{(0)}/n$, where $v_k^{(0)}/n$ is the sample variance of the k th coordinate of \mathbf{X} from CMDS. For the mixing distribution of $\zeta_{i,j}$, we used degrees of freedom $\nu = 5$. These parameter values deliver satisfactory results in the simulation studies, and the same values of the prior parameters are used in all examples unless otherwise specified.

In the random walk Metropolis-Hastings step, the constant multiplier of the variance of the Gaussian proposal density for generating \mathbf{x}_i and σ^2 is chosen based on the characteristics of the data to ensure rapid mixing. Since the number of significant attributes p is often unknown, most examples use $p = 2$ for the purpose of visualization. In the annealed SMC algorithm, we set the number of particles to $K = 200$, the rCESS threshold to $\phi = 0.8$, and the resampling threshold to $\epsilon = 0.5$. Unless otherwise specified in the example, all parameters are sampled during the particle propagation steps. Parallel computation is also implemented for the annealed SMC algorithm with 3 cores across all simulations and examples.

4.1 Experiment 1: Data with known true underlying dimension

We start by investigating the model's performance in selecting the optimal dimension when the true underlying dimension is known within the data. The simulated data consists of 100 random samples of \mathbf{X} drawn from a 5-dimensional multivariate Gaussian distribution with mean 0 and variance I , the identity matrix. The true pairwise dissimilarities $\delta_{i,j}$ from \mathbf{X} are calculated as

$$\delta_{i,j} = \mathcal{D}(\mathbf{x}_i, \mathbf{x}_j), \quad i, j = 1, \dots, n,$$

where the dissimilarity metric \mathcal{D} is chosen to be the Euclidean distance. Given $\delta_{i,j}$, the observed dissimilarities $d_{i,j}$ are generated from a normal distribution with mean $\delta_{i,j}$ and standard deviation of 1. These dissimilarities are truncated at 0. Thus, the simulated data consists of a 100×100 symmetric matrix of dissimilarities calculated from Euclidean distances with Gaussian errors. We included one frequentist method, CMDS, along with two Bayesian methods, MCMC and annealed SMC (ASMC), in the performance evaluation. In ASMC, all three candidate models were considered, and both STRESS values and log marginal likelihood estimates (logM) were reported.

Table 1: A summary of the STRESS values and log marginal likelihood estimates (logM) from applying the different MDS methods. The values in bold are the optimal dimensions selected by the lowest STRESS values or the largest log marginal likelihood estimates. All results are the averages of 20 runs. Bold values indicate the best performance for each case.

p	CMDS STRESS	MCMC STRESS	ASMC					
			$\mathcal{M}_{TN}^{\text{Euclidean}}$		$\mathcal{M}_{TSN}^{\text{Euclidean}}$		$\mathcal{M}_{TT}^{\text{Euclidean}}$	
			STRESS	logM	STRESS	logM	STRESS	logM
2	0.399	0.330	0.396	-5005.763	0.397	-7641.413	0.351	-7291.686
3	0.266	0.268	0.265	-4869.795	0.266	-7454.384	0.246	-7178.706
4	0.184	0.233	0.186	-4535.830	0.188	-7325.840	0.187	-7094.328
5	0.163	0.223	0.168	-4391.146	0.172	-7269.501	0.171	-7010.791
6	0.199	0.232	0.206	-5058.168	0.213	-7803.021	0.201	-7612.594
7	0.238	0.247	0.240	-5491.560	0.246	-7984.964	0.243	-7995.441
8	0.278	0.262	0.274	-6033.348	0.280	-8409.323	0.288	-8689.978

Table 1 displays the STRESS values and log marginal likelihood estimates obtained from various MDS methods. All methods identified the true dimension as 5. Additionally, it can be observed that the candidate model $\mathcal{M}_{TN}^{\text{Euclidean}}$ attained the highest log marginal likelihood estimates and was considered the optimal model as expected.

4.2 Experiment 2: Data with skewed errors

In this example, we test how the proposed model performs when data skewness is present. We generated a dataset consisting of n accurate/unobserved observations $\mathbf{X} = \{\mathbf{x}_1, \dots, \mathbf{x}_n\}$. Each of the observations has a dimension of 20, i.e., $\mathbf{x}_i = (x_{i,1}, \dots, x_{i,20})^\top$. The observations were simulated as a mixture of 50% from $\mathcal{N}(0, 1)$, 25% from $\mathcal{N}(100, 10)$ and 25% from $\mathcal{N}(-10, 1)$. Next, we generated n noisy/observed observations \mathbf{Z} of size 20 through a two-step process. First, we introduced minor errors into all observations \mathbf{X}

with the aim of simulating the systematic errors arising from data measurement. Second, varied percentages of the observations are subject to the contamination of moderate and significant errors, with the intention of replicating the scenario in which some observations are inaccurately recorded during data measurement. Specifically, moderate and significant errors were introduced into 20% and 2% of the observations, respectively. The Euclidean metric was then applied to obtain the dissimilarities $d_{i,j}$'s from the noisy observations \mathbf{Z} and the dissimilarities $\tilde{d}_{i,j}$'s from accurate observations \mathbf{X} . The errors $\epsilon_{i,j}$'s were computed by:

$$\epsilon_{i,j} = d_{i,j} - \tilde{d}_{i,j}, \quad i \neq j, i, j = 1, \dots, n.$$

A detailed description of the data generation process with skewed errors is given in *Supplementary*. We conducted experiments in several scenarios with sample sizes of $n = 100, 300, 500, 700$ to assess the scalability of the model. Each scenario is repeated for 20 runs. A histogram of the errors $\epsilon_{i,j}$'s from one run with $n = 300$ is shown in Figure 2(a). Our goal is to compare the performance of the proposed model $\mathcal{M}_{TSN}^{\text{Euclidean}}$ with the standard model with truncated Gaussian $\mathcal{M}_{TN}^{\text{Euclidean}}$ using the log marginal likelihoods when data are contaminated by some skewed errors.

Figure 2(b) depicts the comparison of the computation times, showing the advantages of the annealed SMC algorithm over the MCMC algorithm across all scenarios with varying sample sizes. We examined four scenarios to compare the performance of the annealed SMC algorithm and the MCMC algorithm under the identical truncated Gaussian model. This comparison helped illustrate how computation time varies with increasing sample size. The computation times typically show greater variability as the sample size increases, as observed for $n = 100, 300$, and 500. In the case of $n = 700$, the narrower boxes are attributed to some incomplete MCMC runs caused by out-of-memory issues. Therefore, we had to restrict the results to successful runs with fewer ASMC and MCMC iterations. These results illustrate that, even with more complicated models such as the truncated skewed Gaussian, our runtime remains comparable and even faster, demonstrating the scalability of the proposed framework to larger datasets. Figure 2(c) shows the performance comparison in terms of the log marginal likelihood as the skewed error presents. The findings of the study demonstrate that the model incorporating a truncated skewed Gaussian exhibits better performance, as the data under consideration is primarily with skewed errors. The results provide evidence that the skewed distributions are necessary for certain circumstances for modeling purposes.

4.3 Experiment 3: Data with outliers

In the following experiment, we use the simulated data to investigate the robustness of the proposed models. The simulated dataset contains 100 observations which are generated from a 10-dimensional multivariate Gaussian distribution with mean 0 and variance I , the identity matrix. The observed dissimilarity matrix is generated by first computing the Euclidean dissimilarities from the raw observations and then adding some Gaussian errors centered around the true Euclidean dissimilarities, with a standard deviation of 0.5. To study the robustness of different models, we added outliers by randomly selecting a different proportion of the observed dissimilarities and doubling their values. We

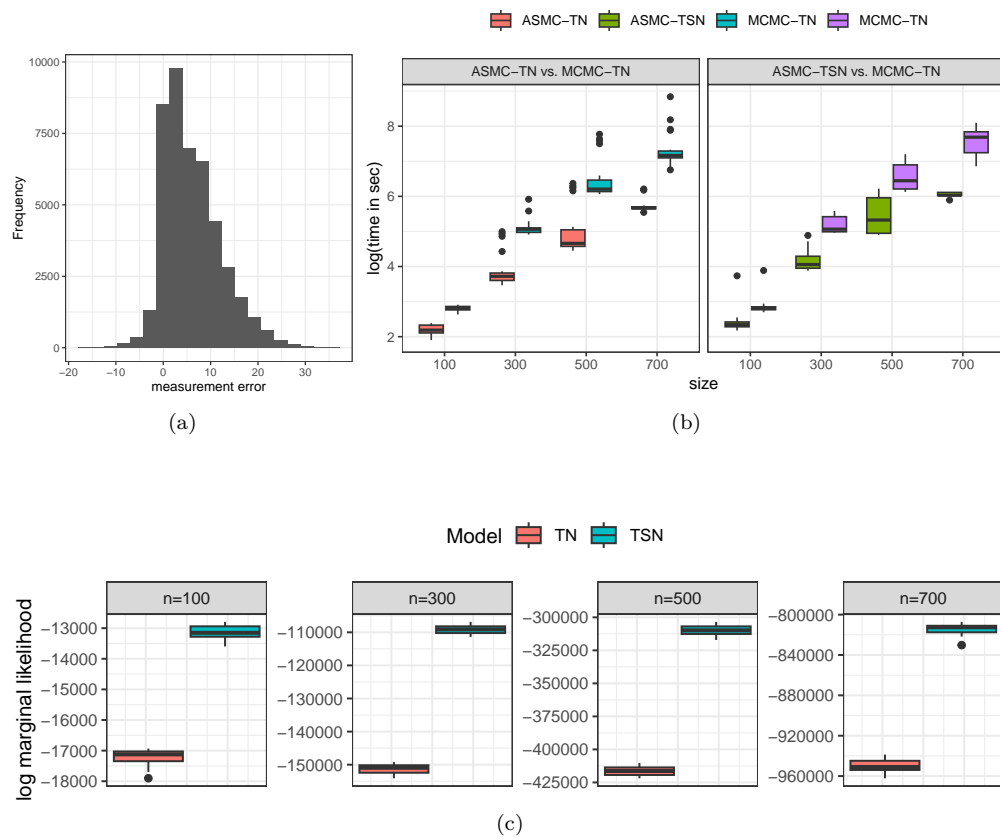


Figure 2: (a) The histogram of the errors with 300 observations. (b) The boxplots of computation times for different models. The computation budget is kept consistent across all comparisons between pairs of Bayesian methods. (c) The boxplots of the log marginal likelihood for different models.

considered two scenarios with varying proportions of outliers in dissimilarities; the first contains 5% outliers, and the second has 15% outliers. Figure 3(a) shows the histograms of the dissimilarity $d_{i,j}$'s under the two scenarios. In scenario 2, the increased percentage of outliers leads to a heavier tail in the dissimilarity histogram. In this simulation, we test the robustness of the models $\mathcal{M}_{TSN}^{\text{Euclidean}}$ and $\mathcal{M}_{TT}^{\text{Euclidean}}$.

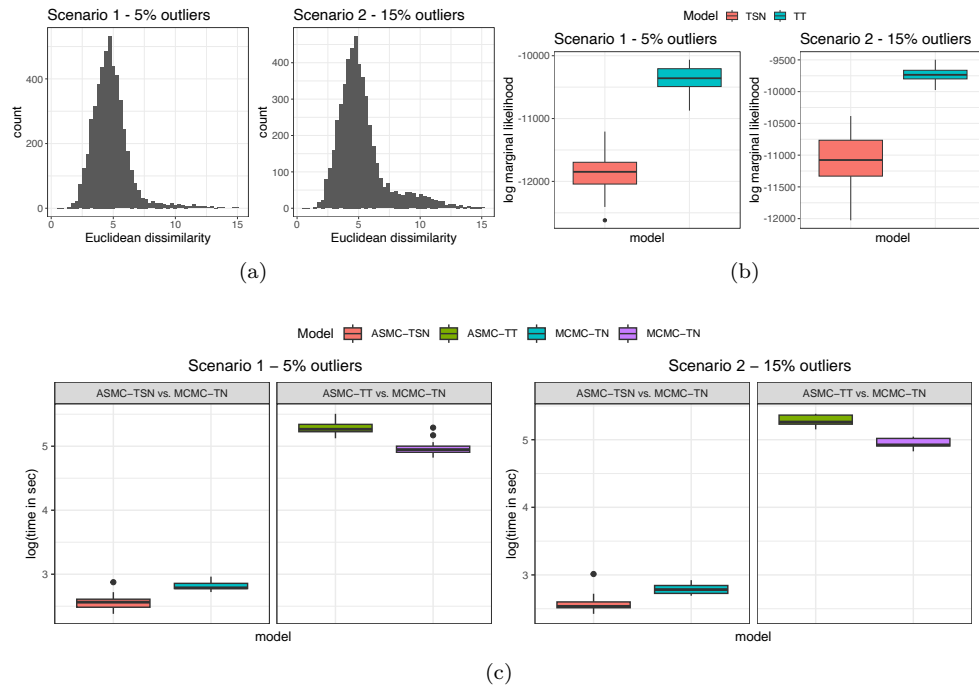


Figure 3: (a) The histograms of the dissimilarity $d_{i,j}$ under Euclidean metrics. The left histogram is from scenario 1, where the data contain 5% outliers. The right histogram is from scenario 2, where the data contain 15% outliers. (b) The boxplots of the log marginal likelihood for different models. Red: $\mathcal{M}_{TSN}^{\text{Euclidean}}$; Blue: $\mathcal{M}_{TT}^{\text{Euclidean}}$. Dimension p is 2. (c) The boxplots of computation times for different models. The computation budget is kept consistent across all comparisons between pairs of Bayesian methods.

Figure 3(b) shows the marginal likelihood in log scale for the two models under the two scenarios. In scenario 1, where the data only contained 5% outliers, the histogram of the dissimilarity does not show an obvious heavy tail. According to the left boxplot in Figure 3(b), the model $\mathcal{M}_{TT}^{\text{Euclidean}}$ is preferred since it produces higher log marginal likelihoods overall. When the percentage of outliers is increased to 15%, an obviously heavier tail can be observed in the right histogram in Figure 3(a). The boxplot on the right in Figure 3(b) indicates that model $\mathcal{M}_{TT}^{\text{Euclidean}}$ is favored, as it yields higher log marginal likelihoods with smaller variability. As the percentage of outliers in the data increases, model $\mathcal{M}_{TSN}^{\text{Euclidean}}$ exhibits greater variance, while model $\mathcal{M}_{TT}^{\text{Euclidean}}$ demonstrates smaller variance across different seeds. Figure 3(c) displays the comparison of

the computation times between the annealed SMC algorithm and the MCMC algorithm across candidate models with different outlier percentages. It is evident that ASMC with $\mathcal{M}_{TSN}^{\text{Euclidean}}$ outperforms MCMC with $\mathcal{M}_{TN}^{\text{Euclidean}}$ in terms of computation time. When comparing ASMC with the more complex model $\mathcal{M}_{TT}^{\text{Euclidean}}$ to MCMC with the simpler model $\mathcal{M}_{TN}^{\text{Euclidean}}$, ASMC still demonstrates comparable runtime.

5 Data Applications

5.1 NIPS text data with incremental dimensions

In the first example, we demonstrate the performance of the adaptive inference with the annealed SMC algorithm on text data with incremental dimensions. The text data is generated from articles from the Conference on Neural Information Processing Systems (NIPS). The NIPS dataset contains NIPS conference papers published between 1987 and 2015 (Dua and Graff, 2017; Perrone et al., 2017). In this study, our focus is directed toward a subset of the NIPS dataset, comprising a matrix of word counts extracted from 55 articles. This matrix is referred to as the document-term matrix, which is constructed after tokenization, stop-word removal, and truncation of the corpus by retaining only words that appear more than fifty times. The document-term matrix has counts for a list of 15005 words. Instead of Euclidean dissimilarity, we consider Cosine dissimilarity, which is suitable for discrete data such as word counts since it measures how dissimilar the documents are irrespective of their sizes.

We fitted the model $\mathcal{M}_{TT}^{\text{Cosine}}$ and compared the results in terms of STRESS values and computational times. The number of significant attributes p is assumed to be 2. In this toy example, we considered the cases with $n_0 = 10, 50$, and $n_1 = 1, 5$. For each combination of n_0 and n_1 , we considered two cases: one applies the annealed SMC algorithm with a fixed dimension to all $n = n_0 + n_1$ observations, while the other employs the annealed SMC algorithm with an incremental dimension, leveraging the results from the first n_0 observations are already known. We set the number of particles to $K = 100$ and the rCESS threshold to $\phi = 0.9$ in this example. At each particle propagation step in the annealed SMC algorithm, a subset of two parameters is randomly selected for updating. If the selected parameter includes $\{\mathbf{x}_1, \dots, \mathbf{x}_n\}$, a random subset containing half of its components is updated. This setting balances computational efficiency with effective exploration of the parameter space.

From Table 2, it can be seen that the STRESS values from both cases are close, and this validates the performance of the annealed SMC algorithm for incremental dimension. For the two cases with $n_0 = 10$, the computation times decrease by an average of 24% when applying the annealed SMC algorithm for incremental dimension. Similarly, for the two cases with $n_0 = 50$, the computation times fall by 31%. Moreover, the variability in computation times decreased in both cases with the implementation of adaptive inference.

Table 2: A summary of the STRESS values and computation times from applying the annealed SMC on GBMDS to observations with different dimensions. The first and third rows present the results from applying the annealed SMC algorithm of fixed dimension to all observations. The results in the second and fourth rows come from running the annealed SMC algorithm of incremental dimension, given the results from n observations are known. The values in the parentheses are the standard deviation of the computation times. All results are the averages of 30 runs.

Observations	STRESS	Time (in sec)	Observations	STRESS	Time (in sec)
$n = 11$	0.7093	19.0 (4.2)	$n = 51$	0.7449	143.0 (36.3)
$n_0 = 10, n_1 = 1$	0.7133	15.1 (3.1)	$n_0 = 50, n_1 = 1$	0.7419	100.9 (13.9)
$n = 15$	0.7194	29.4 (9.9)	$n = 55$	0.7545	156.5 (37.0)
$n_0 = 10, n_1 = 5$	0.6930	21.6 (4.0)	$n_0 = 50, n_1 = 5$	0.7536	104.4 (14.4)

5.2 Geographical data

The second example aims to study the performance of the proposed method and present visualizations of the estimations with uncertainty measures. As an illustrative example to study the performances of the CMDS and BMDS methods, we considered the US cities dataset from the US Census Bureau ([Census Bureau, 2021](#)), which contains Latitude and Longitude information from 15 large US cities. To evaluate the performances of the GBMDS, we appended 10 noise variables to add complexity. These noise variables are generated from a Gaussian distribution with a mean of 0 and variance comparable to the “Latitude” or “Longitude” variables.

We performed experiments across three scenarios, each of which had a distinct set of noises added to the data. The noises are incorporated into the data by assigning varying weights to the true and noisy variables. We represent the signal-to-noise ratio as $R_{s:n}$, which is defined as the ratio of the weight of the true signal to that of the noise. If $R_{s:n} > 1$, it indicates that there is more signal than noise. In the first scenario, we assigned equal importance to all variables, resulting in $R_{s:n} = 1$. In this case, the results depend equally on the signal and noisy variables. In the second scenario, we placed more emphasis on crucial variables such as “Latitude” and “Longitude” by decreasing the weights assigned to redundant noises, setting $R_{s:n} = 4$. In the third scenario, we tested an extreme condition where the majority of the weights were allocated to the “Latitude” and “Longitude” variables, setting $R_{s:n} = 10$. In all experiments, we normalized the weights to ensure they sum up to 1.

We employed two Bayesian methods, MCMC and annealed SMC (ASMC), to implement our proposed GBMDS. To initialize the GBMDS, we utilized the results from CMDS. For simplicity, we assumed $\psi = 0$ to reduce the model to $\mathcal{M}_{TN}^{\text{Euclidean}}$. To ensure a fair comparison between the two Bayesian methods, we kept the computational budget constant. Specifically, we first ran annealed SMC with 300 particles and recorded the number of iterations. We then allocated the same budget to MCMC by setting the number of MCMC iterations equal to the product of the annealed SMC iterations and the number of particles. The purpose of this example is to highlight the advantages of

the Bayesian method over the frequentist method. For small datasets under the same model $\mathcal{M}_{TN}^{\text{Euclidean}}$, it is expected that the two Bayesian methods would provide similar results and MDS reconstructions of city locations, provided we run sufficiently long MCMC iterations in MCMC and use a large number of particles in ASMC. Therefore, we excluded the results from MCMC as both Bayesian methods yield similar results on this small dataset. This exclusion does not affect the overall conclusions, but rather ensures a clearer presentation of the key findings.

Table 3 presents the STRESS values obtained from CMDS and GBMDS with ASMC (GBMDS-ASMC) for the three scenarios. Our analysis indicates that the Bayesian approach yields lower STRESS values across all three scenarios. Figure 4 displays the estimated locations of the 15 US cities obtained by GBMDS-ASMC. Transformations, such as rotation and reflection, were applied to the estimated locations from GBMDS-ASMC to fit the cities' actual geographical locations. One can observe from Figures 4(a) and 4(d) that under the equal weight scenario, several cities are geographically misplaced no matter what transformations are applied. The reason behind this mismatch is that the information in the "Latitude" and "Longitude" variables are masked by the remaining variables. The estimated locations shown in 4(c) and 4(f) lead to a closer match when higher weights are assigned to the "Latitude" and "Longitude" variables.

Table 3: A Summary of the STRESS values for different methods on US City data under scenarios 1 to 3 with different noise-to-signal ratios. Bold values indicate the best performance for each case.

	CMDS	GBMDS-ASMC
Scenario 1: $R_{s:n} = 1$	0.4557	0.3521
Scenario 2: $R_{s:n} = 4$	0.4680	0.3910
Scenario 3: $R_{s:n} = 10$	0.4726	0.4103

The Bayesian approach offers several advantages over the classical approach. In addition to producing smaller STRESS values, the Bayesian approach enables the estimation of uncertainty by leveraging samples from the posterior distribution. To this end, we performed Procrustes transformations on the posterior samples of \mathbf{x}_i to align each sample as closely as possible to the estimated coordinates, effectively standardizing all the posterior samples of \mathbf{x}_i . Using the transformed posterior samples, we constructed credible regions, represented as ellipses in Figures 4(d) to 4(f). In contrast to CMDS, our GBMDS-ASMC method offers uncertainty measures, with tight credible regions in scenarios where the signal-to-noise ratio is high and wider credible regions when more noises exist in the data.

5.3 NIH text data

In this example, we apply the MDS techniques to text data consisting of documents and words. We aim to showcase the application of our proposed method and investigate the effect of dimension p . The dataset holds information on research grants awarded by the National Institutes of Health (NIH) in 2022 (NIH, 2022). The raw data contain

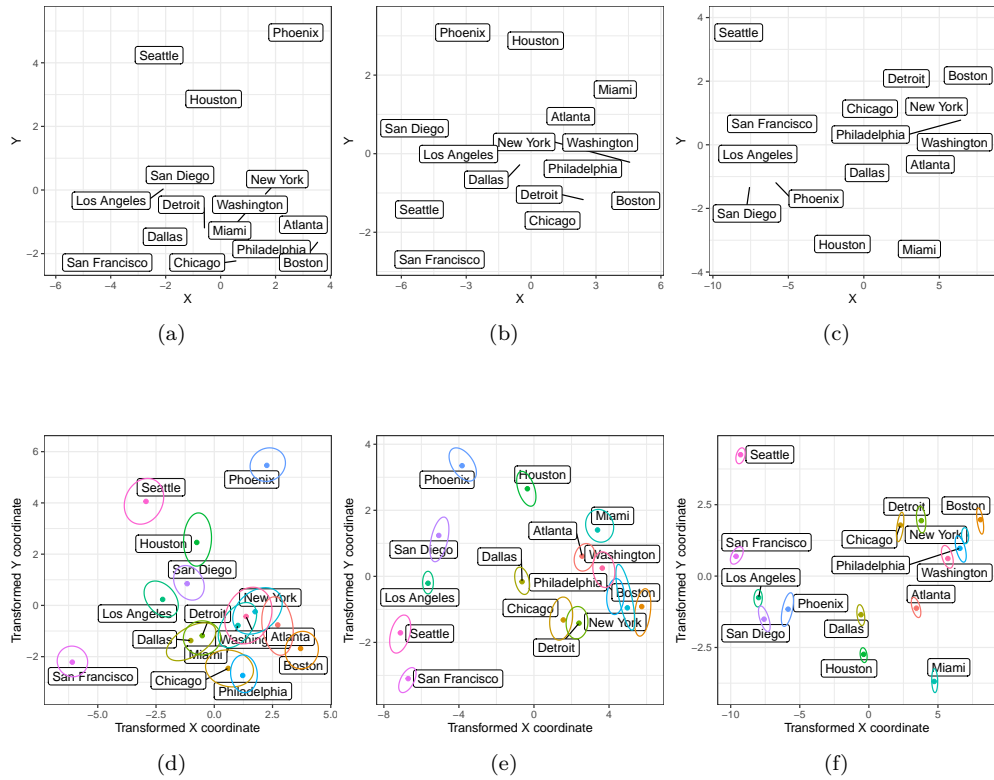


Figure 4: Estimated locations of the 15 US cities from CMDS and GBMDS-ASMC after transformations. Sub-figures (a) to (c) are results from CMDS and (d) to (f) are from GBMDS-ASMC. $R_{sn} = 1$ in (a) and (d), $R_{sn} = 4$ in (b) and (e), $R_{sn} = 10$ in (c) and (f). For GBMDS-ASMC, the ellipses are generated from all the posterior samples with the 95% credible regions. The posterior medians of \mathbf{x}_i 's are served as the estimated coordinates of the 15 US cities in the two-dimensional space.

1471 grant abstracts from Saint Louis in the United States. To preprocess the data, we performed tokenization and removed stop words. This results in a document-term matrix with a dimension of 1471 by 238919, where each row represents an abstract and contains the word counts for all words in that abstract. We then re-weighted the word counts by multiplying an inverse document frequency vector to adjust for the relative importance of words in the entire collection of documents. The purpose of this reweighing step was to account for the varying frequencies of words across documents. We calculated the Cosine dissimilarities of the documents and used them as input to the MDS methods. Figure 5a displays the histogram of Cosine dissimilarity values, with Y-axis on a log scale indicating the log count of occurrences. The histogram shows a spike at the lower end, around 0, and then a gradually increasing trend in counts as the Cosine dissimilarities approach 1. This distribution suggests that the dataset contains pairs with high similarity (values near 0) and high dissimilarity (values near 1), with a notable concentration at higher dissimilarity levels.

We varied the dimension p across values from 2 to 10, as well as 15, 20, 25, 30, 35, and 40, to examine its impact on the results. All four candidate models are included in the comparison. Figure 5b presents the relationship between model dimensionality and log marginal likelihood estimates for four different models, represented by distinct colored markers. Each line represents a different model's performance across dimensions, with log marginal likelihood estimates initially increasing as the dimension rises, reaching a peak around dimensions 8 to 10 for most models, and then slightly decreasing as dimensionality continues to increase. In general, models with higher log marginal likelihood estimates are considered to perform better. In this case, model $\mathcal{M}_{TSN}^{\text{Euclidean}}$ reaches the highest overall log marginal likelihood estimates at dimension $p = 9$, indicating superior performance in higher dimensions. However, model $\mathcal{M}_{TSN}^{\text{Cosine}}$ exhibits a notable advantage in lower dimensions, achieving relatively high log marginal likelihood estimates when p is small. This suggests that while $\mathcal{M}_{TSN}^{\text{Euclidean}}$ is optimal in higher dimensions, $\mathcal{M}_{TSN}^{\text{Cosine}}$ may be more suitable or efficient when the dimensionality is low. Thus, there may be trade-offs between models based on the dimension, with $\mathcal{M}_{TSN}^{\text{Cosine}}$ performing better at lower dimensions and $\mathcal{M}_{TSN}^{\text{Euclidean}}$ excelling as the dimension increases.

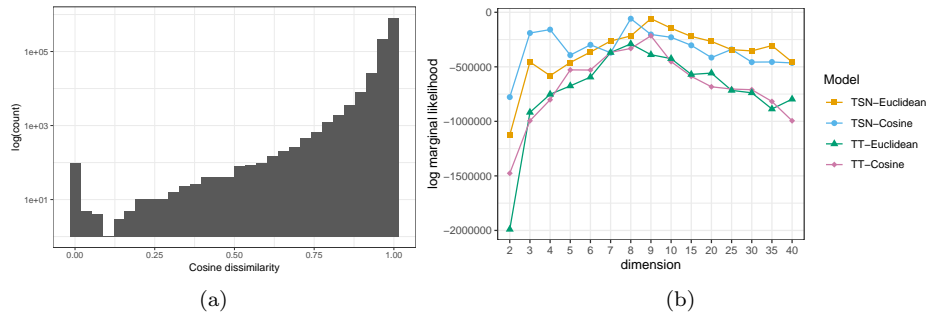


Figure 5: (a) The histogram of Cosine dissimilarity. Counts on Y-axis are in log scale. (b) The log marginal likelihood for different models under varying dimensions.

5.4 Clustering abstract text data

The last example explores an interesting application of MDS, clustering objects by grouping similar observations based on their dissimilarities. With MDS techniques, the coordinates of objects can be represented in a low-dimensional space. Visualizing these clusters in the reduced-dimensional space is of interest, as it can provide meaningful insights into the relationships between the groups. The dataset comprises 139 English abstracts collected from three academic journals during 2022 and 2023: 44 from *Annals of Mathematics*, 50 from *Bayesian Analysis*, and 45 from *Biometrics*. While all three journals focus on the development of statistical and mathematical methods, each emphasizes distinct application areas. This study aims to assess the performance of the proposed model in clustering these abstract texts. We employed the Jaccard metric with a 2-gram model to construct the dissimilarity matrix. A 2-gram model represents a subsequence of two successive elements within an abstract, including words, numbers, or symbols. Each abstract was first treated as a set of unique 2-grams, and the Jaccard dissimilarity was computed based on the intersection and union of these sets. This metric is effective for identifying abstracts with overlapping vocabularies or patterns, mainly when abstracts are dense with technical terms. Additionally, the use of a 2-gram model is beneficial in applications where sequences of words are relevant.

We applied GBMDS-ASMC for reducing dimension, followed by the partition around medoids algorithm (PAM) (Kaufman, 1990) to group the results into 3 clusters. In this study, we predetermined the number of clusters as 3, corresponding to the three journals included in the dataset. All candidate models were evaluated, and the model $\mathcal{M}_{TSN}^{\text{Euclidean}}$ at dimension $p = 7$ achieved the highest log marginal likelihood estimates. Therefore, it was selected as the optimal model for this example. Figure 6 presents the pairwise scatterplots and density plots of the clustering results, highlighting that the first three dimensions contribute significantly to the clustering, with clear separations between clusters. This result provides a meaningful representation of the data, yielding well-defined clusters with visual separation. We also evaluated the classification accuracy as another performance metric using the known journal labels of each abstract. The GBMDS-ASMC method correctly classified all abstracts into their respective journals. Table 4 summarizes the top 20 keywords from each cluster along with their corresponding journals. The results reveal the presence of similar keywords related to the development of statistical and mathematical methods. Additionally, distinct keywords are observed, reflecting the specific application and thematic focus unique to each journal.

6 Conclusion and Discussion

In this work, we introduced a generalized Bayesian multidimensional scaling (GBMDS) framework that addresses the limitations of existing BMDS methods based on MCMC. By incorporating non-Gaussian error distributions and diverse dissimilarity metrics, we enhanced the robustness and flexibility of MDS. We also developed an adaptive ASMC algorithm for efficient Bayesian inference, which provides a nearly unbiased marginal likelihood estimator as a byproduct. This estimator facilitates model comparison across

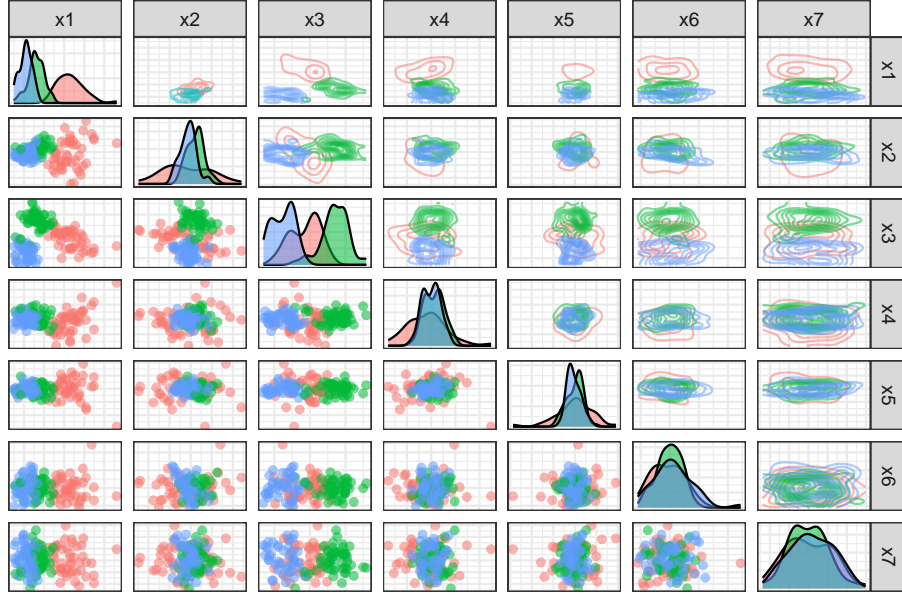


Figure 6: Estimated coordinates of the abstracts obtained using GBMDS-ASMC with $p = 7$. The lower panel displays pairwise scatter plots, the diagonal shows density plots, and the upper panel provides contour plots of the density. The colors indicate three distinct clusters.

Table 4: A summary of the top 20 keywords from each cluster on the abstract data.

Cluster	Keywords	Journal
1	conjecture, prove, theory, smooth, groups, minimal, stable, Euler, symmetric, finite, hypersurfaces, singularity, characteristic, spaces, field, cohomology, Frobenius, algebra, existence, invariant	<i>Annals of Mathematics</i>
2	Bayesian, model, posterior, prior, Gaussian, distribution, inference, Monte-Carlo, spatial, network, linear, MCMC, hierarchical, mixture, predictive, sampling, computational, Dirichlet-process, shrinkage, uncertainty	<i>Bayesian Analysis</i>
3	estimator, treatment, data, effect, regression, causal, randomized, covariate, functional, dose, population, time, consistent, hazards, heterogeneity, confounding, asymptotic, trials, Cox, longitudinal	<i>Biometrics</i>

candidate models with different error distributions, dissimilarity metrics, and dimensions. Our approach was validated using both synthetic and real data, demonstrating its superior computational efficiency, scalability, and robustness compared to traditional MCMC-based methods under the same computational budget.

Bayesian model selection offers several advantages over classical approaches such as p -values and information criteria. First, Bayes factors provide a direct probabilistic measure of model support, making them intuitive even for non-statisticians. Second, Bayesian model selection is consistent, meaning that given enough data, it will asymptotically select the model with the smallest Kullback-Leibler divergence to the true model under mild conditions (Berk, 1966), whereas some classical methods, such as hypothesis testing based on p -values, do not always guarantee consistency. Third, Bayesian model selection naturally penalizes excessive model complexity, favoring simpler models when competing models fit the data similarly (Berger et al., 2001; Robert et al., 2007).

Due to these advantages, we propose selecting the optimal model-dimension combination for GBMDS using Bayes factors. Unlike the simple Bayesian criterion in Oh and Raftery (2001), our fully Bayesian approach directly utilizes the nearly unbiased marginal likelihood estimator from the annealed SMC algorithm with an adaptive annealing scheme, providing a principled and computationally efficient framework for the choice of model and dimension. In contrast, frequentist model selection via STRESS relies on the specifically constructed statistics that are tailored to particular cases, limiting its generalizability. Our approach estimates the marginal likelihood as a byproduct of annealed SMC, eliminating the need for additional computational steps. This efficient estimation procedure not only facilitates robust model comparison across different distance metrics and dimensional choices but also provides a significant computational advantage over existing MCMC-based methods.

The proposed annealed SMC algorithm offers a viable alternative to MCMC, particularly when computational resources are available and faster inference is prioritized over long MCMC chains. Note that the proposed adaptive ASMC framework is highly flexible and can straightforwardly integrate existing MCMC kernels from the literature, including those based on HMC, to further enhance computational efficiency. While memory constraints can arise for high-dimensional particles, dimension reduction methods such as MDS yield low-dimensional latent variables, making memory demands more manageable. Moreover, our method does not require storing the complete history of particles at each annealing step, further reducing memory overhead. As a result, even a personal laptop can efficiently handle a large number of particles. Memory constraints can also be addressed by either increasing the number of SMC iterations while using fewer particles—an approach that has been shown to maintain or even improve performance with proper tuning (Wang et al., 2020)—or by leveraging parallel implementations that distribute the particle set across computing cores. Methods such as entangled Monte Carlo (Jun et al., 2012), the island particle filter (Vergé et al., 2015), and the distributed particle filter (Heine and Whiteley, 2017) enhance scalability, ensuring that memory limitations do not pose a significant barrier to running SMC with a large number of particles.

The proposed method is implemented in an R package GBMDS which can be accessed at <https://github.com/SFU-Stat-ML/GBMDS>. The implementation integrates R

and C++ to enhance computational efficiency, making it more accessible for practitioners. To assess scalability and runtime performance, we compared our implementation with the MCMC-based method in [Oh and Raftery \(2001\)](#) using their available R package BayMDS ([Oh and Lee, 2022](#)) across various simulation studies and data applications. The results indicate that even for more complex models, such as the truncated skewed Gaussian and truncated Student's t , our method achieves comparable or faster runtimes, demonstrating its scalability to larger datasets. When applying the BayMDS package to datasets with over 1,000 observations, we encountered processing limitations due to the requested data size exceeding its computational capacity. This further highlights the practical advantages of our proposed approach in handling large-scale problems.

We have applied Procrustes transformations to the posterior samples to address the non-identifiability issue. The transformed posterior samples were then used to construct credible regions, providing a measure of uncertainty. In the geographical data example, we observed that the credible regions for certain observations were relatively broad, suggesting that specific patterns should be interpreted with caution. Exploring alternative post-processing transformations could further enhance interpretability. Additionally, it would be valuable to investigate how the number of particles in the annealed SMC algorithm affects the credible regions.

There are several directions for future work. Our proposed framework aids in identifying a suitable model for dissimilarities and an optimal p for dimension reduction. While Euclidean models are well-suited for two-dimensional visualization, representing object configurations in a non-Euclidean space remains an open challenge. Future work could explore effective visualization techniques for such structures, improving interpretability in high-dimensional non-Euclidean embeddings. Another important application of MDS is clustering, where observations are grouped based on dissimilarity. In our final data application, we evaluated the proposed model using heuristic clustering methods. However, model-based clustering provides a probabilistic alternative that allows for more rigorous classification and uncertainty quantification. Building on [Oh and Raftery \(2007\)](#), one could extend the adaptive annealed SMC algorithm to jointly perform MDS and model-based clustering, providing a fully Bayesian treatment of clustering assignments. This extension could also apply to text clustering, where carefully chosen dissimilarity metrics define meaningful cluster structures. Additionally, future work could focus on enhancing the efficiency of the annealed SMC algorithm. One straightforward approach is to integrate existing MCMC kernels from the BMDS literature into ASMC for comparison. Another promising direction is subsampling-based inference ([Gunawan et al., 2020](#)), which can reduce computational costs while maintaining accuracy. Furthermore, advanced parallelization strategies could significantly improve scalability, enabling the proposed method to accommodate increasingly large datasets.

Supplementary Material

Supplementary Materials to “Generalized Bayesian Multidimensional Scaling and Model Comparison”. Supplementary materials include a document with the details of the dissimilarity metrics, details of the particle propagation step, and details of the data-generating process in simulation studies.

References

Bakker, R. and Poole, K. T. (2013). “Bayesian metric multidimensional scaling.” *Political Analysis*, 21(1): 125–140. [2](#)

Berger, J. O., Pericchi, L. R., Ghosh, J., Samanta, T., De Santis, F., Berger, J., and Pericchi, L. (2001). “Objective Bayesian methods for model selection: Introduction and comparison.” *Lecture Notes-Monograph Series*, 135–207. [31](#)

Berk, R. H. (1966). “Limiting behavior of posterior distributions when the model is incorrect.” *The Annals of Mathematical Statistics*, 37(1): 51–58. [31](#)

Borg, I. and Groenen, P. J. (2005). *Modern multidimensional scaling: Theory and applications*. Springer Science & Business Media. [2](#)

Bronstein, A. M., Bronstein, M. M., and Kimmel, R. (2006). “Generalized multidimensional scaling: a framework for isometry-invariant partial surface matching.” *Proceedings of the National Academy of Sciences*, 103(5): 1168–1172. [3](#)

Census Bureau, U. S. (2021). “United States Census Bureau: Data & Map.” URL <https://www.census.gov/data.html> [25](#)

Chib, S. and Jeliazkov, I. (2001). “Marginal likelihood from the Metropolis–Hastings output.” *Journal of the American Statistical Association*, 96(453): 270–281. [10](#)

Chopin, N. and Papaspiliopoulos, O. (2020). *An Introduction to Sequential Monte Carlo*. Springer Series in Statistics. Springer International Publishing. URL <https://link.springer.com/10.1007/978-3-030-47845-2> [3](#)

Dai, C., Heng, J., Jacob, P. E., and Whiteley, N. (2022). “An Invitation to Sequential Monte Carlo Samplers.” *Journal of the American Statistical Association*, 117(539): 1587–1600. URL <https://doi.org/10.1080/01621459.2022.2087659> [3](#)

Del Moral, P., Doucet, A., and Jasra, A. (2006). “Sequential Monte Carlo samplers.” *Journal of the Royal Statistical Society: Series B (Statistical Methodology)*, 68(3): 411–436. [3](#), [11](#), [13](#)

— (2007). “Sequential Monte Carlo for Bayesian Computation.” *Bayesian Statistics*, 8: 1–34. [11](#)

— (2012). “An adaptive sequential Monte Carlo method for approximate Bayesian computation.” *Statistics and Computing*, 22: 1009–1020. [3](#)

Douc, R. and Cappé, O. (2005). “Comparison of resampling schemes for particle filtering.” In *ISPA 2005. Proceedings of the 4th International Symposium on Image and Signal Processing and Analysis, 2005.*, 64–69. IEEE. [14](#)

Doucet, A., Briers, M., and Sénécal, S. (2006). “Efficient block sampling strategies for sequential Monte Carlo methods.” *Journal of Computational and Graphical Statistics*, 15(3): 693–711. [3](#)

Doucet, A., De Freitas, N., Gordon, N. J., et al. (2001). *Sequential Monte Carlo methods in practice*, volume 1. Springer. [3](#)

Doucet, A. and Johansen, A. M. (2009). “A tutorial on particle filtering and smoothing: Fifteen years later.” *Handbook of Nonlinear Filtering*, 12(656-704): 3. [3](#)

Dua, D. and Graff, C. (2017). “UCI Machine Learning Repository.” URL <http://archive.ics.uci.edu/ml> [24](#)

Fan, Y., Wu, R., Chen, M.-H., Kuo, L., and Lewis, P. O. (2011). “Choosing among partition models in Bayesian phylogenetics.” *Molecular Biology and Evolution*, 28(1): 523–532. [11](#)

Goodall, C. (1991). “Procrustes methods in the statistical analysis of shape.” *Journal of the Royal Statistical Society: Series B (Methodological)*, 53(2): 285–321. [11](#)

Gronau, Q. F. and Lee, M. D. (2020). “Bayesian inference for multidimensional scaling representations with psychologically interpretable Metrics.” *Computational Brain & Behavior*, 3(3): 322–340. [2](#)

Gunawan, D., Dang, K.-D., Quiroz, M., Kohn, R., and Tran, M.-N. (2020). “Subsampling sequential Monte Carlo for static Bayesian models.” *Statistics and Computing*, 30(6): 1741–1758. [32](#)

Han, C. and Carlin, B. P. (2001). “Markov chain Monte Carlo methods for computing Bayes factors: A comparative review.” *Journal of the American Statistical Association*, 96(455): 1122–1132. [3](#)

Heine, K. and Whiteley, N. (2017). “Fluctuations, stability and instability of a distributed particle filter with local exchange.” *Stochastic Processes and their Applications*, 127(8): 2508–2541.

URL <https://www.sciencedirect.com/science/article/pii/S0304414916302137> [31](#)

Holbrook, A. J., Lemey, P., Baele, G., Dellicour, S., Brockmann, D., Rambaut, A., and Suchard, M. A. (2020). “Massive parallelization boosts big Bayesian multidimensional scaling.” *Journal of Computational and Graphical Statistics*, 1–14. [2](#)

Jaccard, P. (1901). “Étude comparative de la distribution florale dans une portion des Alpes et des Jura.” *Bull Soc Vaudoise Sci Nat*, 37: 547–579. [3](#)

Jeffreys, H. (1935). “Some tests of significance, treated by the theory of probability.” In *Mathematical Proceedings of the Cambridge Philosophical Society*, volume 31, 203–222. Cambridge University Press. [3](#)

Jun, S.-h., Wang, L., and Bouchard-côté, A. (2012). “Entangled Monte Carlo.” In Pereira, F., Burges, C., Bottou, L., and Weinberger, K. (eds.), *Advances in Neural Information Processing Systems*, volume 25. Curran Associates, Inc.

URL https://proceedings.neurips.cc/paper_files/paper/2012/file/dc4c44f624d600aa568390f1f1104aa0-Paper.pdf [31](#)

Kass, R. E. and Raftery, A. E. (1995). “Bayes factors.” *Journal of the American Statistical Association*, 90(430): 773–795. [10](#)

Kaufman, L. (1990). “Partitioning around medoids (program pam).” *Finding groups in data*, 344: 68–125. [29](#)

Kong, A. (1992). “A note on importance sampling using standardized weights.” *University of Chicago, Dept. of Statistics, Tech. Rep*, 348. [14](#)

Kruskal, J. B. (1964). “Multidimensional scaling by optimizing goodness of fit to a nonmetric hypothesis.” *Psychometrika*, 29(1): 1–27. [11](#)

Lange, K. L., Little, R. J., and Taylor, J. M. (1989). “Robust statistical modeling using the t distribution.” *Journal of the American Statistical Association*, 84(408): 881–896. [7](#)

Li, B. and Han, L. (2013). “Distance weighted Cosine similarity measure for text classification.” In *International Conference on Intelligent Data Engineering and Automated Learning*, 611–618. Springer. [3](#)

Lin, L. and Fong, D. K. (2019). “Bayesian multidimensional scaling procedure with variable selection.” *Computational Statistics & Data Analysis*, 129: 1–13. [2](#), [7](#)

Liu, B., Lubold, S., Raftery, A. E., and McCormick, T. H. (2024). “Bayesian hyperbolic multidimensional scaling.” *Journal of Computational and Graphical Statistics*, 33(3): 869–882. [2](#)

Mémoli, F. (2011). “Gromov–Wasserstein distances and the metric approach to object matching.” *Foundations of Computational Mathematics*, 11(4): 417–487. [3](#)

Neal, R. M. (2001). “Annealed importance sampling.” *Statistics and Computing*, 11(2): 125–139. [11](#)

Neal, R. M. et al. (2011). “MCMC using Hamiltonian dynamics.” *Handbook of Markov chain Monte Carlo*, 2(11): 2. [2](#)

NIH (2022). “National Institutes of Health ExPORTER.” URL <https://reporter.nih.gov/exporter/abstracts> [26](#)

Oh, M.-S. and Lee, E.-K. (2022). “BayMDS: An R Package for Bayesian Multidimensional Scaling and Choice of Dimension.” *Applied Psychological Measurement*, 46(3): 250. [19](#), [32](#)

Oh, M.-S. and Raftery, A. E. (2001). “Bayesian multidimensional scaling and choice of dimension.” *Journal of the American Statistical Association*, 96(455): 1031–1044. [2](#), [5](#), [6](#), [16](#), [18](#), [19](#), [31](#), [32](#)

— (2007). “Model-based clustering with dissimilarities: A Bayesian approach.” *Journal of Computational and Graphical Statistics*, 16(3): 559–585. [2](#), [32](#)

Perrone, V., Jenkins, P. A., Spano, D., and Teh, Y. W. (2017). “Poisson random fields for dynamic feature models.” *Journal of Machine Learning Research*, 18. [24](#)

Robert, C. P. and Wraith, D. (2009). “Computational methods for Bayesian model choice.” In *AIP Conference Proceedings*, volume 1193, 251–262. American Institute of Physics. [10](#)

Robert, C. P. et al. (2007). *The Bayesian choice: from decision-theoretic foundations to computational implementation*, volume 2. Springer. [31](#)

Skilling, J. (2004). “Nested sampling.” In *AIP Conference Proceedings*, volume 735, 395–405. American Institute of Physics. 10

Torgerson, W. S. (1952). “Multidimensional scaling: I. Theory and method.” *Psychometrika*, 17(4): 401–419. 2, 5

Vergé, C., Dubarry, C., Del Moral, P., and Moulines, E. (2015). “On parallel implementation of sequential Monte Carlo methods: the island particle model.” *Statistics and Computing*, 25(2): 243–260.

URL <https://doi.org/10.1007/s11222-013-9429-x> 31

Wang, L., Wang, S., and Bouchard-Côté, A. (2020). “An annealed sequential Monte Carlo method for Bayesian phylogenetics.” *Systematic Biology*, 69(1): 155–183. 3, 10, 11, 16, 31

Wang, S., Ge, S., Doig, R., and Wang, L. (2021). “Adaptive semiparametric Bayesian differential equations via sequential Monte Carlo.” *Journal of Computational and Graphical Statistics*, 1–14. 3

Zhou, Y., Johansen, A. M., and Aston, J. A. (2016). “Toward automatic model comparison: an adaptive sequential Monte Carlo approach.” *Journal of Computational and Graphical Statistics*, 25(3): 701–726. 3, 16

Supplementary Materials to “Generalized Bayesian Multidimensional Scaling and Model Comparison”

1 Distance (Dissimilarity) Metric

In this section, we will formally define the metric space and introduce several dissimilarity metrics that are used in the paper. Let M be a set and let \mathcal{D} be a real-valued function defined on the Cartesian product $M \times M$ satisfying:

1. $\mathcal{D}(x, y) \geq 0, \forall x, y \in M;$
2. $\mathcal{D}(x, y) = 0 \iff x = y;$
3. $\mathcal{D}(x, y) = \mathcal{D}(y, x), \forall x, y \in M;$
4. $\mathcal{D}(x, z) \leq \mathcal{D}(x, y) + \mathcal{D}(y, z), \forall x, y, z \in M.$

Then the function \mathcal{D} is considered as a metric or dissimilarity function in M , and the set M together with \mathcal{D} is called a metric space. We will denote a vector in \mathbb{R}^q in bold when $q > 1$ and refer to its scalar components by subscripts. For instance, let $\mathbf{x} \in \mathbb{R}^q$ be a vector with $\mathbf{x} = (x_1, \dots, x_q)^\top$ representing the values of q attributes. We consider the following dissimilarity metrics on \mathbb{R}^q :

- Euclidean metric (L^2 norm): $\mathcal{D}(\mathbf{x}, \mathbf{y}) = \|\mathbf{x} - \mathbf{y}\|_2 = \sqrt{\sum_{i=1}^q (x_i - y_i)^2}$.
- Cosine metric: $\mathcal{D}(\mathbf{x}, \mathbf{y}) = 1 - \left(\sum_{i=1}^q x_i y_i \right) / \left(\sqrt{\sum_{i=1}^q x_i^2} \sqrt{\sum_{i=1}^q y_i^2} \right)$. The Cosine metric is used in the case of text analysis, as word frequencies are non-negative, the Cosine metric ranges from 0 to 1.
- Jaccard metric: $\mathcal{D}(\mathbf{x}, \mathbf{y}) = 1 - |\mathbf{x} \cap \mathbf{y}| / |\mathbf{x} \cup \mathbf{y}|$. The Jaccard metric is used in the case of text analysis to measure the dissimilarity between two documents, and the metric ranges from 0 to 1. Here, \mathbf{x} and \mathbf{y} represent two documents with text, $|\mathbf{x} \cap \mathbf{y}|$ is the number of words common to both documents, and $|\mathbf{x} \cup \mathbf{y}|$ is the number of words across both documents.

The present work exclusively incorporates the Euclidean, Cosine and Jaccard metrics. Nonetheless, the proposed methods have the potential for application across a broader range of dissimilarity metrics.

2 Conditional posterior distributions in the particle propagation step

In this section, we describe the conditional posterior distributions for the parameters. In each conditional posterior distribution, we use $|\dots$ to denote conditioning on the data and all other parameters and/or indicators.

- The full conditional distribution for v is

$$\lambda_k | \cdots \sim IG(\alpha + n/2, \beta_k + \tau_r s_k/2), \quad (1)$$

where s_k/n is the sample variance of the k th coordinates of \mathbf{x}_i 's

- The full conditional posterior distributions of $\{\mathbf{x}_{1:n}\}$ and σ^2 are

$$\begin{aligned} \gamma_r(\{\mathbf{x}_{1:n}\} | \cdots, \mathcal{M}_{TSN}) \propto & \exp \left\{ -\tau_r \left(\frac{1}{2\sigma^2} \text{SSR} \right. \right. \\ & + \frac{m}{2} \log \left(\sigma^2 (F_{\delta_{i,j}, \sigma, \psi}(U) - F_{\delta_{i,j}, \sigma, \psi}(0)) \right) \\ & \left. \left. - \sum_{i>j} \log \left(\Phi \left(\psi \frac{d_{i,j} - \delta_{i,j}}{\sigma} \right) \right) + \frac{1}{2} \sum_{i=1}^n \mathbf{x}_i^\top \Lambda^{-1} \mathbf{x}_i \right) \right\}, \end{aligned} \quad (2)$$

$$\begin{aligned} \gamma_r(\{\mathbf{x}_{1:n}\} | \cdots, \mathcal{M}_{TT}) \propto & \exp \left\{ -\tau_r \left(\frac{1}{2\sigma^2} \sum_{i>j} \zeta_{i,j} (d_{i,j} - \delta_{i,j})^2 \right. \right. \\ & + \sum_{i>j} \log \left(\Phi \left(\frac{(U - \delta_{i,j}) \sqrt{\zeta_{i,j}}}{\sigma} \right) - \Phi \left(-\frac{\delta_{i,j} \sqrt{\zeta_{i,j}}}{\sigma} \right) \right) \\ & \left. \left. + \frac{1}{2} \sum_{i=1}^n \mathbf{x}_i^\top \Lambda^{-1} \mathbf{x}_i \right) \right\}, \end{aligned} \quad (3)$$

where $\text{SSR} = \sum_{i>j} (d_{i,j} - \delta_{i,j})^2$, $F(\cdot)$ is the cdf of skewed Gaussian distribution, $\Phi(\cdot)$ is the standard Gaussian cdf, and $m = n(n-1)/2$ is the total number of dissimilarities for n objects.

$$\begin{aligned} \gamma_r(\sigma^2 | \cdots, \mathcal{M}_{TSN}) \propto & \sigma^{-2(a+1)} \exp \left\{ -\tau_r \left(\frac{1}{2\sigma^2} \text{SSR} \right. \right. \\ & + \frac{m}{2} \log \left(\sigma^2 (F_{\delta_{i,j}, \sigma, \psi}(U) - F_{\delta_{i,j}, \sigma, \psi}(0)) \right) \\ & \left. \left. - \sum_{i>j} \log \left(\Phi \left(\psi \frac{d_{i,j} - \delta_{i,j}}{\sigma} \right) \right) + \frac{b}{\sigma^2} \right) \right\}, \end{aligned} \quad (4)$$

$$\begin{aligned}
\gamma_r(\sigma^2 | \dots, \mathcal{M}_{TT}) \propto \sigma^{-m} \exp \left\{ -\tau_r \left(\frac{1}{2\sigma^2} \sum_{i>j} \zeta_{i,j} (d_{i,j} - \delta_{i,j})^2 \right. \right. \\
\left. \left. + \sum_{i>j} \log \left(\Phi \left(\frac{(U - \delta_{i,j}) \sqrt{\zeta_{i,j}}}{\sigma} \right) - \Phi \left(\frac{-\delta_{i,j} \sqrt{\zeta_{i,j}}}{\sigma} \right) \right) + \frac{b}{\sigma^2} \right) \right\}.
\end{aligned} \tag{5}$$

The full conditional posterior distributions of $\{\mathbf{x}_{1:n}\}$ and σ^2 do not admit closed forms, a random walk Metropolis-Hastings step is implemented with the Gaussian proposal densities. The full conditional posterior distribution of ψ also does not have a closed form. A random walk Metropolis-Hastings step with Gaussian proposal density is applied. At iteration r , we perform the following steps:

1. Propose new variates with Gaussian proposals:

$$\begin{aligned}
\{\mathbf{x}_{1:n}\}_* &\sim N(\{\mathbf{x}_{1:n}\}_{r-1}, c\sigma_{r-1}^2/(n-1)), \\
\sigma_*^2 &\sim N(\sigma_{r-1}^2, \sigma_{\sigma_{r-1}^2}^2), \\
\psi_* &\sim N(\psi_{r-1}, 0.1^2),
\end{aligned}$$

where c is a constant multiplier and $\sigma_{\sigma_{r-1}^2}^2$ is the variance of $IG(a+m/2, b+SSR/2)$ distribution.

2. Compute the Metropolis-Hastings Ratio:

$$r_{MH} = \min \left\{ 1, \frac{\gamma_r(\{\mathbf{x}_{1:n}\}_*, \sigma_*^2, \psi_* | \dots)}{\gamma_r(\{\mathbf{x}_{1:n}\}_{r-1}, \sigma_{r-1}^2, \psi_{r-1} | \dots)} \right\}.$$

3. Generate $u \sim \text{Uniform}(0, 1)$ distribution:

- If $u \leq r_{MH}$, then accept $\{\mathbf{x}_{1:n}\}_*, \sigma_*^2, \psi_*$. Set $\{\mathbf{x}_{1:n}\}_r = \{\mathbf{x}_{1:n}\}_*, \sigma_r^2 = \sigma_*^2, \psi_r = \psi_*$.
- If $u > r_{MH}$, then reject $\{\mathbf{x}_{1:n}\}_*, \sigma_*^2, \psi_*$. Set $\{\mathbf{x}_{1:n}\}_r = \{\mathbf{x}_{1:n}\}_{r-1}, \sigma_r^2 = \sigma_{r-1}^2, \psi_r = \psi_{r-1}$.

- For model \mathcal{M}_{TT} , the full conditional distribution for $\zeta_{i,j}$ is

$$\zeta_{i,j} | \dots, \mathcal{M}_{TT} \sim \text{Gamma}((\tau_r + \nu)/2, \tau_r(d_{i,j} - \delta_{i,j})^2/(2\sigma^2) + \nu/4). \tag{6}$$

3 Data generation process for Skewed Measurement Errors

This section details the data-generating process for Experiment 2 in the simulation studies. We generated n accurate/unobserved observations $\mathbf{X} = \{\mathbf{x}_1, \dots, \mathbf{x}_n\}$ of size 20. These accurate observations were simulated as a combination of 50% from $\mathcal{N}(0, 1)$, 25% from $\mathcal{N}(100, 10)$ and 25% from $\mathcal{N}(-10, 1)$. The noisy/observed observations $\mathbf{Z} = \{\mathbf{z}_1, \dots, \mathbf{z}_n\}$ were simulated by successively adding two types of artificial measurement

errors to the accurate observations \mathbf{X} . First, we added some errors corresponding to some systematic errors that occur during data measurement. For example, some measures are always higher than the actual values. We incorporated this information into the accurate observations by adding measurement errors simulated from $\mathcal{N}(0, 1)$. The second type of error reflects the nature that a few observations are mistakenly recorded and deviate from the truth by a significant amount. These observations are treated as outliers. Outliers are introduced using a Categorical random variable $C_i \sim \text{Cat}(1, \mathbf{p})$, $i = 1, \dots, n$, $\mathbf{p} = (p_1, p_2, 1 - p_1 - p_2)$, with p_1 and p_2 corresponding to outliers' percentages. In the simulation, we studied the performance of the proposed model, and we set $p_1 = 0.05$ and $p_2 = 0.02$. Observations were generated as follows:

- When $C_i = 1$, the observation is contaminated by moderate measurement error: measurement errors are generated from $\mathcal{N}(10, 1)$ and added to the observation
- When $C_i = 2$, the observation is contaminated by large measurement error: measurement errors are generated from $\mathcal{N}(20, 1)$ and added to the observation
- When $C_i = 3$, the observation is not contaminated

The Euclidean metric was then applied to obtain the dissimilarities $d_{i,j}$'s from the noisy observations $\mathbf{Z} = \{\mathbf{z}_1, \dots, \mathbf{z}_n\}$ and the dissimilarities $\tilde{d}_{i,j}$'s from accurate measurements $\mathbf{X} = \{\mathbf{x}_1, \dots, \mathbf{x}_n\}$, respectively. The measurement errors $\epsilon_{i,j}$'s were computed by:

$$\epsilon_{i,j} = d_{i,j} - \tilde{d}_{i,j}, \quad i \neq j, \quad i, j = 1, \dots, n. \quad (1)$$

We repeated the process for $n = 100, 300, 500$. The histograms of $d_{i,j}$'s, $\tilde{d}_{i,j}$'s and $\epsilon_{i,j}$'s from one simulation of $n = 300$ are displayed in Figure 1. We can see that the measurement errors do not necessarily follow the Gaussian distribution, and the distribution of the observed dissimilarities is skewed.

Figure 1: (a) Histogram of the observed dissimilarities $d_{i,j}$'s. (b) Histogram of the true dissimilarities $\tilde{d}_{i,j}$'s. (c) Histogram of the measurement errors $\epsilon_{i,j}$'s.

